DISCUSSION

This study shows the positive correlation between the Val^{247} β_2GPI allele and anti-β_2GPI antibody production in a Japanese population, confirming the correlation observed in a British Caucasian population in our previous report (15). A positive correlation between the Val^{247} allele and the presence of anti-β_2GPI antibodies was also reported in Asian American (26) and Mexican patients (27). However, this correlation was not observed in other American populations (26) or in patients with thrombosis or pregnancy complications in the UK (28). This discrepancy may be the result of the difference in the frequency of the Val^{247} allele among races, or the difference in the background of investigated patients. Another possibility is that the relationship between the Val^{247} allele and thrombosis in Caucasians may be controversial due to underpowered studies or to differences in the procedure used to detect anti-β_2GPI antibodies. Methods for the detection of anti-β_2GPI antibodies differ among laboratories. For example, cardiolipin-coated plates or oxygenated plates are used in some methods, whereas unoxygenated plates are used in others. In addition, bovine β_2GPI is used instead of human β_2GPI in some assays. The antibodies used for standardization also differ, although monoclonal antibodies such as EY2C9 and HCAL (29) have been proposed as international standards of calibration materials.

β_2GPI is a major target antigen for aCL, and, according to our previous investigation, B cell epitopes reside in domain IV and are considered to be cryptic and to appear only when β_2GPI interacts with negatively charged surfaces such as cardiolipin, phosphatidylserine, or polyoxygenated polystyrene surface (7), although other studies indicate that the B cell epitopes are located on domain I (13) or domain V (14). According to another interpretation for the specificity of aCL, increment of the local antigen density on the negatively charged surface also contributes to anti-β_2GPI detection in ELISA (8,30). Studies on the crystal structure of human β_2GPI revealed that the lysine-rich site and an extended C-terminal loop region on domain V are crucial for phospholipid binding. Position 247 is located at the N-terminal side of domain V, and, around this position, Lys^{242}, Ala^{243}, and Ser^{244} were suggested to play a role in the interaction between domains IV and V (9,23,31).

Although the Val/Leu^{247} polymorphism may not be very critical for the autoantibody binding, the amino acid substitution at this point was revealed to affect the affinity of monoclonal aCL established from patients with APS and that of purified IgG from patients positive for β_2GPI-dependent aCL. We conformationally optimized to domain V and the domain IV–V complex of β_2GPI variants at position 247, referring the crystal structure of β_2GPI. IgG aCL was screened using the standardized aCL ELISA, in which both the Leu^{247} and the Val^{247} allele of β_2GPI are contained as antigen. Although biochemical characteristics and structure are similar between valine and leucine, the replacement of Leu^{247} by Val^{247} leads to a significant alteration in the tertiary structure of domain V and/or the domain IV–V interaction (Figure 4). It is likely that the structural alteration affects the affinity between anti-β_2GPI autoantibodies and the epitope(s) present on its molecule. One explanation for this phenomenon is that this β_2GPI polymorphism affects the electrostatic interaction between domain IV and domain V or the protein–protein interaction, resulting in differences in the accessibility of the recognition site by the autoantibodies, or the local density of β_2GPI.

Another possible explanation of the correlation between the Val/Leu^{247} polymorphism of β_2GPI and anti-β_2GPI antibodies is T cell reactivity. Ito et al (32) investigated T cell epitopes of patients with anti-β_2GPI autoantibodies by stimulating patients' PBMCs with a peptide library that covers the β_2GPI sequence. Four of 7 established CD4+ T cell clones reacted to peptide fragments that include amino acid position 244–264, then position 247 is included among the candidate epitopes. Arai et al (33) found preferred recognition of peptide position 276–290 by T cell clones from patients with APS. They also found high reactivity to peptide 247–261 in one patient. We speculate that a small alteration in the conformation arising from the valine/leucine substitution at position 247 may affect the susceptibility to generate autoreactive T cell clones in patients with APS.

Our results in this study indicate that the Val/Leu^{247} polymorphism affects the antigenicity of β_2GPI for anti-β_2GPI autoantibodies, and that the Val^{247} allele can be a risk factor for having autoantibodies against this molecule. Therefore, the Val/Leu^{247} variation of β_2GPI may be crucial for autoimmune reactivity against β_2GPI. We further show the significance of the Val/Leu^{247} polymorphism of β_2GPI in the strength of the binding between β_2GPI and anti-β_2GPI autoantibodies. The significance of antigen polymorphisms in the production of autoantibodies or in the development of autoimmune diseases is not well understood. To our knowledge, this report is the first to present a genetic polymorphism of

autoantigen directly affecting its interaction with autoantibodies.

REFERENCES

1. Hughes GR. The antiphospholipid syndrome: ten years on. Lancet 1993;342:341–4.
2. Hughes GR, Harris EN, Gharavi AE. The anticardiolipin syndrome. J Rheumatol 1986;13:486–9.
3. Harris EN, Gharavi AE, Hughes GR. Anti-phospholipid antibodies. Clin Rheum Dis 1985;11:591–609.
4. Galli M, Comfurius P, Maassen C, Hemker HC, de Baets MH, van Breda-Vriesman PJ, et al. Anticardiolipin antibodies (ACA) directed not to cardiolipin but to a plasma protein cofactor. Lancet 1990;335:1544–7.
5. McNeil HP, Simpson RJ, Chesterman CN, Krilis SA. Anti-phospholipid antibodies are directed against a complex antigen that includes a lipid-binding inhibitor of coagulation: β_2-glycoprotein I (apolipoprotein H). Proc Natl Acad Sci U S A 1990;87:4120–4.
6. Matsuura E, Igarashi Y, Fujimoto M, Ichikawa K, Koike T. Anticardiolipin cofactor(s) and differential diagnosis of autoimmune disease. Lancet 1990;336:177–8.
7. Matsuura E, Igarashi Y, Yasuda T, Triplett DA, Koike T. Anticardiolipin antibodies recognize β_2-glycoprotein I structure altered by interacting with an oxygen modified solid phase surface. J Exp Med 1994;179:457–62.
8. Roubey RA, Eisenberg RA, Harper MF, Winfield JB. "Anticardiolipin" autoantibodies recognize β_2-glycoprotein I in the absence of phospholipid: importance of Ag density and bivalent binding. J Immunol 1995;154:954–60.
9. Schwarzenbacher R, Zeth K, Diederichs K, Gries A, Kostner GM, Laggner P, et al. Crystal structure of human β_2-glycoprotein I: implications for phospholipid binding and the antiphospholipid syndrome. EMBO J 1999;18:6228–39.
10. Sanghera DK, Kristensen T, Hamman RF, Kamboh MI. Molecular basis of the apolipoprotein H (β_2-glycoprotein I) protein polymorphism. Hum Genet 1997;100:57–62.
11. Yasuda S, Tsutsumi A, Chiba H, Yanai H, Miyoshi Y, Takeuchi R, et al. β_2-glycoprotein I deficiency: prevalence, genetic background and effects on plasma lipoprotein metabolism and hemostasis. Atherosclerosis 2000;152:337–46.
12. Igarashi M, Matsuura E, Igarashi Y, Nagae H, Ichikawa K, Triplett DA, et al. Human β_2-glycoprotein I as an anticardiolipin cofactor determined using mutants expressed by a baculovirus system. Blood 1996;87:3262–70.
13. Iverson GM, Victoria EJ, Marquis DM. Anti-β_2 glycoprotein I (β_2GPI) autoantibodies recognize an epitope on the first domain of β_2GPI. Proc Natl Acad Sci U S A 1998;95:15542–6.
14. Wang MX, Kandiah DA, Ichikawa K, Khamashta M, Hughes G, Koike T, et al. Epitope specificity of monoclonal anti-β_2-glycoprotein I antibodies derived from patients with the antiphospholipid syndrome. J Immunol 1995;155:1629–36.
15. Atsumi T, Tsutsumi A, Amengual O, Khamashta MA, Hughes GR, Miyoshi Y, et al. Correlation between β_2-glycoprotein I valine/leucine^{247} polymorphism and anti-β_2-glycoprotein I antibodies in patients with primary antiphospholipid syndrome. Rheumatology (Oxford) 1999;38:721–3.
16. Matsuura E, Igarashi Y, Fujimoto M, Ichikawa K, Suzuki T, Sumida T, et al. Heterogeneity of anticardiolipin antibodies defined by the anticardiolipin cofactor. J Immunol 1992;148:3885–91.
17. Atsumi T, Ieko M, Bertolaccini ML, Ichikawa K, Tsutsumi A, Matsuura E, et al. Association of autoantibodies against the phosphatidylserine–prothrombin complex with manifestations of the antiphospholipid syndrome and with the presence of lupus anticoagulant. Arthritis Rheum 2000;43:1982–93.
18. Wilson WA, Gharavi AE, Koike T, Lockshin MD, Branch DW, Piette JC, et al. International consensus statement on preliminary classification criteria for definite antiphospholipid syndrome: report of an international workshop. Arthritis Rheum 1999;42:1309–11.
19. Tan EM, Cohen AS, Fries JF, Masi AT, McShane DJ, Rothfield NF, et al. The 1982 revised criteria for the classification of systemic lupus erythematosus. Arthritis Rheum 1982;25:1271–7.
20. Ichikawa K, Khamashta MA, Koike T, Matsuura E, Hughes GR. β_2-glycoprotein I reactivity of monoclonal anticardiolipin antibodies from patients with antiphospholipid syndrome. Arthritis Rheum 1994;37:1453–61.
21. Matsuura E, Igarashi M, Igarashi Y, Nagae H, Ichikawa K, Yasuda T, et al. Molecular definition of human β_2-glycoprotein I (β_2-GPI) by cDNA cloning and inter-species differences of β_2-GPI in alternation of anticardiolipin binding. Int Immunol 1991;3:1217–21.
22. Matsuura E, Igarashi Y, Yasuda T, Triplett DA, Koike T. Anticardiolipin antibodies recognize β_2-glycoprotein I structure altered by interacting with an oxygen modified solid phase surface. J Exp Med 1994;179:457–62.
23. Bouma B, de Groot PG, van den Elsen JM, Ravelli RB, Schouten A, Simmelink MJ, et al. Adhesion mechanism of human β_2-glycoprotein I to phospholipids based on its crystal structure. EMBO J 1999;18:5166–74.
24. Brooks BR, Bruccoleri RE, Olafson BD, States DJ. CHARMm: a program for macromolecular energy, minimization, and dynamics calculations. J Comput Chem 1983;4:187–217.
25. Carlson W, Karplus M, Haber E. Construction of a model for the three-dimensional structure of human renal renin. Hypertension 1985;7:13–26.
26. Hirose N, Williams R, Alberts AR, Furie RA, Chartash EK, Jain RI, et al. A role for the polymorphism at position 247 of the β_2-glycoprotein I gene in the generation of anti-β_2-glycoprotein I antibodies in the antiphospholipid syndrome. Arthritis Rheum 1999;42:1655–61.
27. Prieto GA, Cabral AR, Zapata-Zuñiga M, Simón AJ, Villa AR, Alarcon-Segovia D, et al. Valine/valine genotype at position 247 of the β_2-glycoprotein I gene in Mexican patients with primary antiphospholipid syndrome: association with anti-β_2-glycoprotein I antibodies. Arthritis Rheum 2003;48:471–4.
28. Camilleri RS, Mackie IJ, Humphries SE, Machin SJ, Cohen H. Lack of association of β_2-glycoprotein I polymorphisms Val247Leu and Trp316Ser with antiphospholipid antibodies in patients with thrombosis and pregnancy complications. Br J Haematol 2003;120:1066–72.
29. Ichikawa K, Tsutsumi A, Atsumi T, Matsuura E, Kobayashi S, Hughes GR, et al. A chimeric antibody with the human γ1 constant region as a putative standard for assays to detect IgG β_2-glycoprotein I–dependent anticardiolipin and anti-β_2-glycoprotein I antibodies. Arthritis Rheum 1999;42:2461–70.
30. Tincani A, Spatola L, Prati E, Allegri F, Ferremi P, Cattaneo R, et al. The anti-β_2-glycoprotein I activity in human anti-phospholipid syndrome sera is due to monoreactive low-affinity autoantibodies directed to epitopes located on native β_2-glycoprotein I and preserved during species' evolution. J Immunol 1996;157:5732–8.
31. Saxena A, Gries A, Schwarzenbacher R, Kostner GM, Laggner P, Prassl R. Crystallization and preliminary x-ray crystallographic studies on apolipoprotein H (β_2-glycoprotein-I) from human plasma. Acta Crystallogr D Biol Crystallogr 1998;54:1450–2.
32. Ito H, Matsushita S, Tokano Y, Nishimura H, Tanaka Y, Fujisao S, et al. Analysis of T cell responses to the β_2-glycoprotein I-derived peptide library in patients with anti-β_2-glycoprotein I antibody-associated autoimmunity. Hum Immunol 2000;61:366–77.
33. Arai T, Yoshida K, Kaburagi J, Inoko H, Ikeda Y, Kawakami Y, et al. Autoreactive CD4+ T-cell clones to β_2-glycoprotein I in patients with antiphospholipid syndrome: preferential recognition of the major phospholipid-binding site. Blood 2001;98:1889–96.

International Immunology, Vol. 17, No. 4, pp. 421–427
doi:10.1093/intimm/dxh221

$CD25^+CD4^+$ regulatory T cells exert *in vitro* suppressive activity independent of CTLA-4

Hiroshi Kataoka[1,2], Shigekazu Takahashi[1], Kan Takase[1], Sho Yamasaki[1,3], Tadashi Yokosuka[1,3], Takao Koike[2] and Takashi Saito[1,3]

[1]Department of Molecular Genetics, Graduate School of Medicine, Chiba University, 1-8-1 Inohana, Chuo-ku, Chiba 260-8670, Japan
[2]Department of Medicine II, Hokkaido University Graduate School of Medicine, N15, W7, Kita-ku, Sapporo 060-8638, Japan
[3]Laboratory for Cell Signaling, RIKEN Research Center for Allergy and Immunology, 1-7-22 Suehirocho, Tsurumi-ku, Yokohama, Kanagawa 230-0045, Japan

Keywords: co-stimulation, *Foxp3*, homeostasis, thymocyte, tolerance

Abstract

Cytotoxic T lymphocyte antigen-4 (CTLA-4) is constitutively expressed on $CD25^+CD4^+$ regulatory T cells (Treg) and is suggested to play a role in Treg-mediated suppression. However, the results of analysis with anti-CTLA-4 have been controversial. We addressed this issue by analyzing mice over-expressing or deficient in CTLA-4. For over-expression, CTLA-4 transgenic mice expressing a full-length (FL) or a truncated (TL) mutant of CTLA-4 were analyzed. FL T cells expressed similar levels of CTLA-4 to Treg, whereas TL T cells expressed much higher levels on the cell surface. The number of Treg in both mice was decreased, although *Foxp3* expression was not altered. Treg from both mice exerted suppressive activity, whereas $CD25^-$ T cells from FL mice showed no suppression. Furthermore, $CD25^+CD4$ thymocytes from young CTLA-4-deficient mice were analyzed and found to exhibit suppressive activity. These results indicate that Treg exert *in vitro* suppressive activity independent of CTLA-4 expression.

Introduction

Cytotoxic T lymphocyte antigen-4 (CTLA-4) is an inhibitory co-stimulation receptor of T cells that mediates the inhibition of T cell activation. As CTLA-4 shares its ligands (CD80 and CD86) with CD28 and has much higher affinity for the ligands than CD28, a low expression of CTLA-4 mediates strong inhibition. Whereas CD28 is constitutively expressed, CTLA-4 is induced only upon TCR stimulation. CTLA-4 inhibits T cell activation by competing with CD28 for ligand binding to block the positive co-stimulation and the delivery of inhibitory signals (1–3). The inhibitory function of CTLA-4 is evidenced by the finding that CTLA-4-deficient ($^-/^-$) mice develop lymphoproliferative disease and become moribund at several weeks of age (4). These observations indicate that CTLA-4 down-regulates T cell activation and maintains peripheral tolerance *in vivo*.

Naturally occurring $CD25^+CD4^+$ regulatory T cells (Treg) suppress self-reactive $CD25^-$ T cells to prevent the development of autoimmunity *in vivo* (5, 6). Treg down-regulate the proliferation of $CD25^-$ T cells upon TCR stimulation *in vitro* in an antigen-non-specific manner, although Treg activation is antigen specific (7). The Treg-mediated suppression requires cell contact and is not mediated by cytokines such as IL-10, IFNγ and tissue growth factor-β (7–9). Treg develop in the thymus and migrate to the periphery (10, 11). Approximately 5% of $CD4^+CD8^-$ [CD4 single positive (SP)] thymocytes are $CD25^+$, and $CD25^+CD4SP$ cells have suppressive property *in vitro*. Neonatal thymectomy causes various organ-specific autoimmune diseases in normal mice due to the reduced number of Treg in the periphery (12). The adoptive transfer of $CD25^-CD4SP$ cells into athymic mice has resulted in the development of similar disorders (13). These studies reveal that Treg differentiate in the thymus and maintain natural self-tolerance.

It has been shown that Treg constitutively express CTLA-4 (14), glucocorticoid-induced tumor necrosis factor receptor (GITR) (15, 16) and CD103, and the Fab fragment of anti-CTLA-4 abrogates the *in vitro* suppressive activity of Treg. Normal mice treated with high doses of anti-CTLA-4 or a mixture of anti-CTLA-4 and anti-CD25 develop autoimmune gastritis. The administration of anti-CTLA-4 reverses the Treg-mediated inhibition of $CD25^-$ T cell-induced colitis *in vivo* (17). These findings suggest that the engagement (or blockade) of

Correspondence to: T. Saito; E-mail: saito@rcai.riken.jp

Transmitting editor: S. Koyasu

Received 28 October 2004, *accepted* 14 January 2005

Advance Access publication 21 February 2005

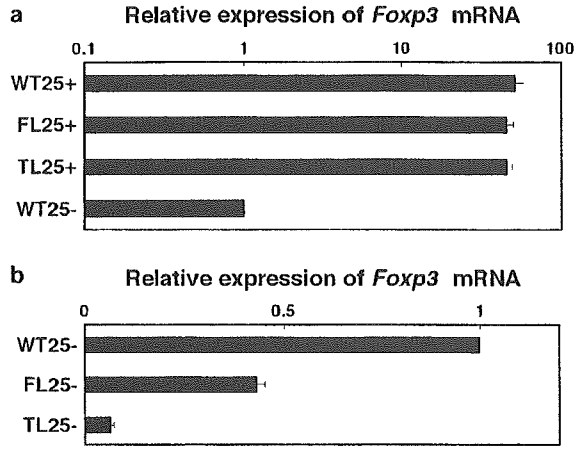

Fig. 1. *Foxp3* mRNA expression in T cells from CTLA-4 Tg mice. (a) *Foxp3* expression in Treg. *Foxp3* mRNA expression in Treg from WT, FL and TL mice was analyzed by real-time PCR in triplicate, normalized to that of β-actin and presented as the ratio to the expression level in $CD25^-CD4^+$ T cells from WT ($WT25^-$). (b) *Foxp3* expression in $CD25^-CD4^+$ T cells. The same analysis as (a) for $CD25^-CD4^+$ T cells. Data are representative of two experiments.

CTLA-4 is involved in the Treg-mediated suppression *in vitro* and the maintenance of self-tolerance *in vivo*. In contrast to these studies, however, anti-CTLA-4 was found to unsuccessfully reverse the *in vitro* suppression in other studies (7, 18), and therefore, the role of CTLA-4 in Treg remains controversial.

Recently, *forkhead box P3* (*Foxp3*) has been shown to be specifically expressed in and essential for the development of Treg. A mutation in *Foxp3* results in a lethal lymphoproliferative disorder in mice (scurfy) (19) as well as humans (immune dysregulation polyendocrinopathy enteropathy X-linked syndrome [IPEX]) (20). The transduction of *Foxp3* into $CD25^-CD4^+$ T cells leads to the up-regulation of CTLA-4 as well as CD25 and the conversion into Treg (21).

Here, we intended to clarify the requirement of CTLA-4 for Treg function by analyzing mice with no expression (knockout mice) or over-expression [transgenic (Tg) mice] of CTLA-4. The results demonstrate that CTLA-4 is not required by Treg to exert *in vitro* suppressive activity.

Methods

Mice

C57BL/6 mice were purchased from SLC Inc. (Shizuoka, Japan). $CTLA\text{-}4^{-/-}$ mice were provided by Tak Mak (University of Toronto, Toronto, Canada). CTLA-4 Tg mice were generated by injecting the inserts of constructs with the human CD2 promoter (22) and a full-length (FL) or a truncated [tail-less (TL)] CTLA-4 cDNA (six amino acids remain in TL) (23) into fertilized eggs of C57BL/6 mice. Two of each Tg founder were obtained and backcrossed onto $CTLA\text{-}4^{-/-}$ mice with the C57BL/6 background (24).

Antibodies and reagents

All cells were grown in RPMI 1640 (Sigma, St Louis, MO, USA) supplemented with 10% heat-inactivated FCS (Sigma), 100 U ml^{-1} penicillin, 100 μg ml^{-1} streptomycin, 50 μM 2-mercaptoethanol (WAKO, Osaka, Japan), 0.1 mM non-essential amino acids and 1 mM sodium pyruvate (Invitrogen Corp., Carlsbad, CA, USA). FITC-conjugated antibodies for $I\text{-}A^b$ and CD4 were purchased from BD PharMingen (San Diego, CA, USA), and FITC–anti-B220, FITC–anti-CD8, PE anti-CD25, biotinylated mAbs for CD8α, CTLA-4 and CD103, allophycocyanin–CD4 and–streptavidin (SA) were from eBioscience (San Diego, CA, USA). Anti-CD3 (145-2C11) and anti-GITR (DTA-1) were provided by J. Bluestone (University of California–San Francisco, San Francisco, CA, USA) and S. Sakaguchi (Kyoto University, Kyoto, Japan), respectively. 5,6-Carboxyfluorescein diacetate succinimyl ester (CFSE) was purchased from Molecular Probes (Eugene, OR, USA).

Cell preparation

$CD25^+$ and $CD25^-CD4^+$ T cells were isolated from spleen and lymph node cells by staining with a mixture of mAbs (FITC-conjugated anti-$I\text{-}A^b$, anti-B220, anti-CD8 and PE–anti-CD25), followed by incubation with anti-FITC beads. The flow through from a MACS column (Miltenyi Biotec, Auburn, CA, USA) was incubated with anti-PE beads and $CD25^+$ cells were separated using MACS. The purities of $CD25^+CD4^+$ and $CD25^-CD4^+$ cells were >94 and 99%, respectively. For $CD25^+CD4SP$ thymocytes, single-cell suspensions from thymi of 10- to 12-day old mice were stained with FITC–anti-CD4, PE–anti-CD25 and biotin–anti-CD8, and then with SA beads, followed by magnetic separation using MACS. $CD25^+$ cells were then sorted by FACS Aria (BD Bioscience, San Jose, CA, USA). These thymocytes contained ~10–20% $CD25^-$ cells and 10% $CD25^+CD4^-CD8^-$ cells. Erythrocyte-depleted irradiated (3500 rad) whole splenocytes were used as antigen presenting cells (APC). In cell division analysis, $CD25^-CD4^+$ T cells from wild-type (WT) mice were labeled with 2 μg ml^{-1} CFSE in 2% FCS-containing RPMI for 8 min at 37°C.

Fig. 2. Suppressive activity of $CD25^+$ and $CD25^-CD4^+$ T cells from CTLA-4 Tg mice. (a) Surface expression of CTLA-4 on $CD25^+$ and $CD25^-CD4^+$ T cells from WT, FL and TL mice. Cells were stained with biotinylated anti-CTLA-4 and SA–APC. (b) Proliferation of $CD25^+$ or $CD25^-CD4^+$ T cells from CTLA-4 Tg mice. Left panel: 2×10^4 $CD25^+$ or $CD25^-CD4^+$ T cells from WT (open bar), FL (hatched bar) and TL (closed bar) mice were cultured with 8×10^4 APC in the presence of 1 μg ml^{-1} anti-CD3 at 37°C for 72 h. Right panel: the same culture was stimulated with 10 ng ml^{-1} phorbol myristate acetate + 1 μM ionomycin at 37°C for 72 h. (c) Suppressive activity of Treg from CTLA-4 Tg mice. Graded numbers of Treg from WT (squares), FL (triangles) and TL (circles) mice were cultured with 2×10^4 $CD25^-CD4^+$ responder T cells in the presence of 1 μg ml^{-1} anti-CD3 and 8×10^4 APC. (d) Suppressive activity of non-regulatory $CD25^-CD4^+$ T cells from CTLA-4 Tg mice on proliferation of responder T cells. Graded numbers of Treg from WT ($WT25^+$; closed squares) mice or $CD25^-CD4^+$ T cells from WT ($WT25^-$, open squares), FL ($FL25^-$, open triangles) and TL ($TL25^-$, open circles) mice were cultured with 2×10^4 responder T cells in the presence of 1 μg ml^{-1} anti-CD3 and 8×10^4 APC. (e) Inhibition of responder T cell division by $CD25^+$ or $CD25^-CD4^+$ T cells from CTLA-4 Tg mice. A total of 2×10^4 CFSE-labeled $CD25^-CD4^+$ responder T cells were cultured with $WT25^+$, $WT25^-$, $FL25^-$ and $TL25^-$ in the presence of 1 μg ml^{-1} anti-CD3 and 8×10^4 APC. Data are representative of three experiments.

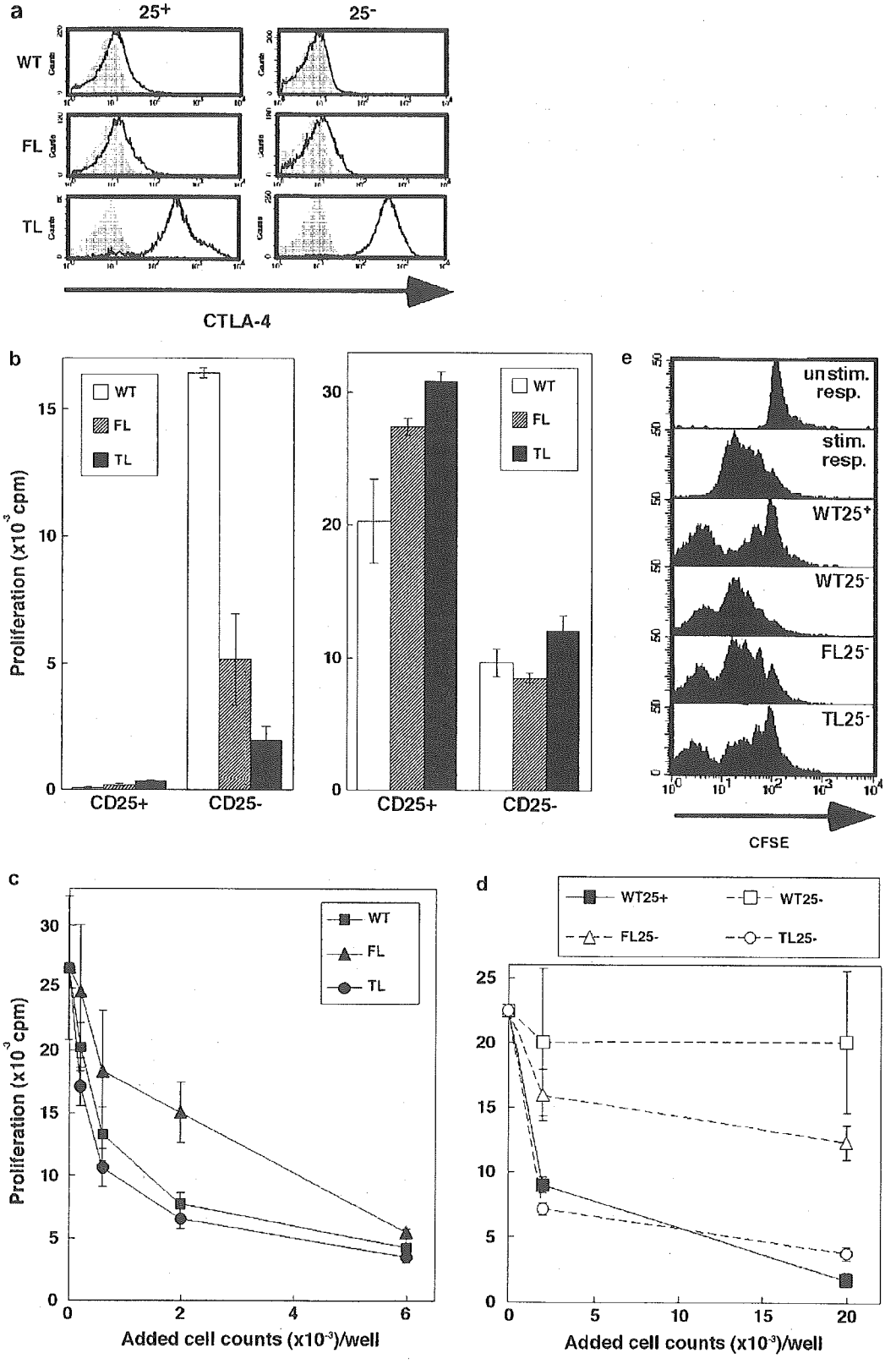
a
25+
25-
WT
FL
TL
CTLA-4
b
WT
FL
TL
Proliferation (x10-3 cpm)
CD25+
CD25-
e
unstim. resp.
stim. resp.
WT25+
WT25-
FL25-
TL25-
CFSE
c
Added cell counts (x10-3)/well
d
WT25+
WT25-
FL25-
TL25-
Added cell counts (x10-3)/well

Real-time PCR

Total RNA was extracted using an RNeasy Mini Kit (Qiagen, Valencia, CA, USA). *Foxp3* mRNA expression levels were quantified by real-time PCR using an ABI PRISM 7000 (Applied Biosystems, Foster City, CA, USA) and *Foxp3* primers (5'-GGG GCC CAC ACC TCT TCT TCC T-3' and 5'-GGC TGA TCA TGG CTG GGT TGT CC-3'). Cycling conditions were 50°C for 2 min, 95°C for 10 min and 40 cycles of 95°C for 30 s, 60°C for 30 s and 72°C for 30 s. Relative *Foxp3* mRNA expression in each population was determined by normalizing to that of β-actin, and presented as the ratio to the expression level of $CD25^-CD4^+$ T cells from WT mice.

Proliferation assay

A total of 2×10^4 $CD25^-CD4^+$ responder T cells were cultured with 8×10^4 APC and graded numbers of sorted $CD25^+CD4^+$ or $CD25^-CD4^+$ T cells and 1 or 10 μg ml^{-1} anti-CD3 at 37°C for 72 h. Tritiated thymidine incorporation during the last 8–10 h of the culture was measured. For cell division analysis, CFSE-labeled $CD25^-CD4^+$ T cells were cultured with various populations for 72 h and analyzed by flow cytometry.

Results

Over-expression of CTLA-4 did not alter Foxp3 mRNA expression in Treg

Tg mice expressing FL and truncated (TL) forms of CTLA-4 under the control of the CD2 promoter were established (24) and crossed with CTLA-$4^{-/-}$ mice. Analysis of splenic T cells showed that $CD25^+CD4^+$ Treg in both Tg mice were reduced in number. $CD25^+$ T cells constituted 2.1 ± 1.1% of $CD4^+$ T cells from FL Tg mice and 1.6 ± 1.0% from TL Tg mice, whereas WT C57BL/6 mice contained 9.0 ± 2.0%. As *Foxp3* is correlated with Treg development (21), *Foxp3* mRNA expression in $CD25^+CD4^+$ and $CD25^-CD4^+$ T cells from both Tg mice ($FL25^+/25^-$ and $TL25^+/25^-$, respectively) was examined. $FL25^+$ and $TL25^+$ cells expressed similar levels of *Foxp3* mRNA to WT Treg (Fig. 1a). Whereas *Foxp3* mRNA expression was much lower in $WT25^-$ cells than in Treg, it was significantly reduced in $FL25^-$ and $TL25^-$ cells reciprocally to the CTLA-4 expression (Fig. 1b). These results indicate that CTLA-4 neither enhances *Foxp3* mRNA expression in $CD25^+$ T cells nor induces it in $CD25^-$ T cells.

Over-expression of CTLA-4 did not affect suppressive activity of Treg

Despite the decrease in the number of Treg, both FL and TL mice did not develop any lymphoproliferative diseases (24), suggesting that the decrease in the number of Treg is sufficient for suppressing self-reactive T cells. Therefore, we examined the suppressive activity of Treg from Tg mice by isolating Treg by cell sorting. The surface expression of CTLA-4 on $FL25^+$ cells was similar to that on Treg, whereas the expression was much higher on $TL25^+$ cells (Fig. 2a) due to the lack of adaptor protein complex-2 (AP2)-mediated endocytosis (23). CTLA-4 was constitutively expressed also on $CD25^-CD4^+$ T cells from FL ($FL25^-$) or TL ($TL25^-$) mice, both of which were as hypo-responsive to TCR stimulation as Treg (Fig. 2b). Moreover, $FL25^-$ and $TL25^-$ cells exhibited lower responses to TCR stimulation reciprocally to the expression level of CTLA-4 (Fig. 2b). When $CD25^-$ T cells were mixed with $CD25^+$ T cells for the analysis of the *in vitro* suppressive activity, both $FL25^+$ cells and $TL25^+$ cells exhibited suppression similar to $WT25^+$ cells (Fig. 2c). These findings indicate that the cytoplasmic tail of CTLA-4 is dispensable for the Treg-mediated suppression and that the expression level of CTLA-4 does not determine the extent of the suppression.

Constitutive expression of the physiological level of CTLA-4 on $CD25^-$ T cells did not induce suppressive activity

We then examined whether the constitutive expression of CTLA-4 induced suppressive activity in non-regulatory $CD25^-$ T cells. Although $FL25^-$ cells expressed similar levels of surface CTLA-4 to Treg, they did not show any significant suppressive activity compared with Treg (Fig. 2d). In contrast, $TL25^-$ cells that expressed much higher levels of CTLA-4 than Treg exerted as strong a suppressive activity as Treg. We further analyzed the cell division of CFSE-labeled responder T cells to determine the influence of $FL25^-$ or $TL25^-$ cells on the responder T cells. As shown in Fig. 2(e), $WT25^+$ cells and not $FL25^-$ cells strongly inhibited the responder T cell division. In contrast, $TL25^-$ cells delayed the division to the same extent as that of $WT25^+$ cells. These results confirm that the suppressive activity of Treg does not depend on the expression of CTLA-4, although an extremely high expression of CTLA-4 can provide non-Treg with suppressive activity.

$CD25^+CD4SP$ thymocytes from young CTLA-$4^{-/-}$ mice exert in vitro suppressive activity

An analysis of the suppressive activity of Treg from CTLA-$4^{-/-}$ mice would obviously provide an answer to the question of whether CTLA-4 is required for the Treg-mediated suppression. Peripheral $CD4^+$ T cells showed the activation phenotype in CTLA-$4^{-/-}$ mice (4). Indeed, ~30 and 10% of splenic $CD4^+$ T cells expressed CD25 in young CTLA-$4^{-/-}$ and normal mice,

Fig. 3. Suppressive activity of $CD25^+$CD4 SP thymocytes from young CTLA-$4^{-/-}$ mice. (a) Normal thymocyte development in young CTLA-$4^{-/-}$ mice. Thymocytes from 10- to 12-day old CTLA-4+/+, +/− and −/− mice were stained with anti-CD4 allophycocyanin and anti-CD8 FITC. (b) Expression of CTLA-4, GITR and CD103 on the cell surface of thymocytes from 10- to 12-day old CTLA-$4^{-/-}$ mice. Thymocytes were stained with anti-CD4 allophycocyanin, PE–anti-CD25 and biotinylated anti-CTLA-4, anti-GITR or anti-CD103. $CD25^+CD4$ thymocytes were gated and analyzed for CTLA-4 (upper panels), GITR (middle panels) and CD103 (bottom panels). (c) $CD25^+$ CD4 SP thymocytes from young CTLA-$4^{-/-}$ mice are hypo-responsive. A total of 1×10^4 $CD25^+$ CD4 SP thymocytes from 10- to 12-day old CTLA-these changes result in "$CD25^+$ CD4 SP thymocytes"+/+, +/− and −/− mice were cultured in the presence of 10 μg ml^{-1} anti-CD3 and 4×10^4 APC. (d) Suppressive activity of $CD25^+$ CD4 SP thymocytes from 10- to 12-day old CTLA-$4^{-/-}$ mice. A total of 2×10^4 adult $CD25^-$ responder T cells were cultured with graded numbers of $CD25^+CD4SP$ (+/+, closed triangles; +/−, closed diamonds; −/−, closed circles), $CD25^-CD4$ SP (+/+, open triangles; +/−, open diamonds; −/−, open circles) or adult T cells ($CD25^+$, closed squares; $CD25^-$, open squares) in the presence of 10 μg ml^{-1} soluble anti-CD3 and 8×10^4 APC. Data are representative of five independent experiments.

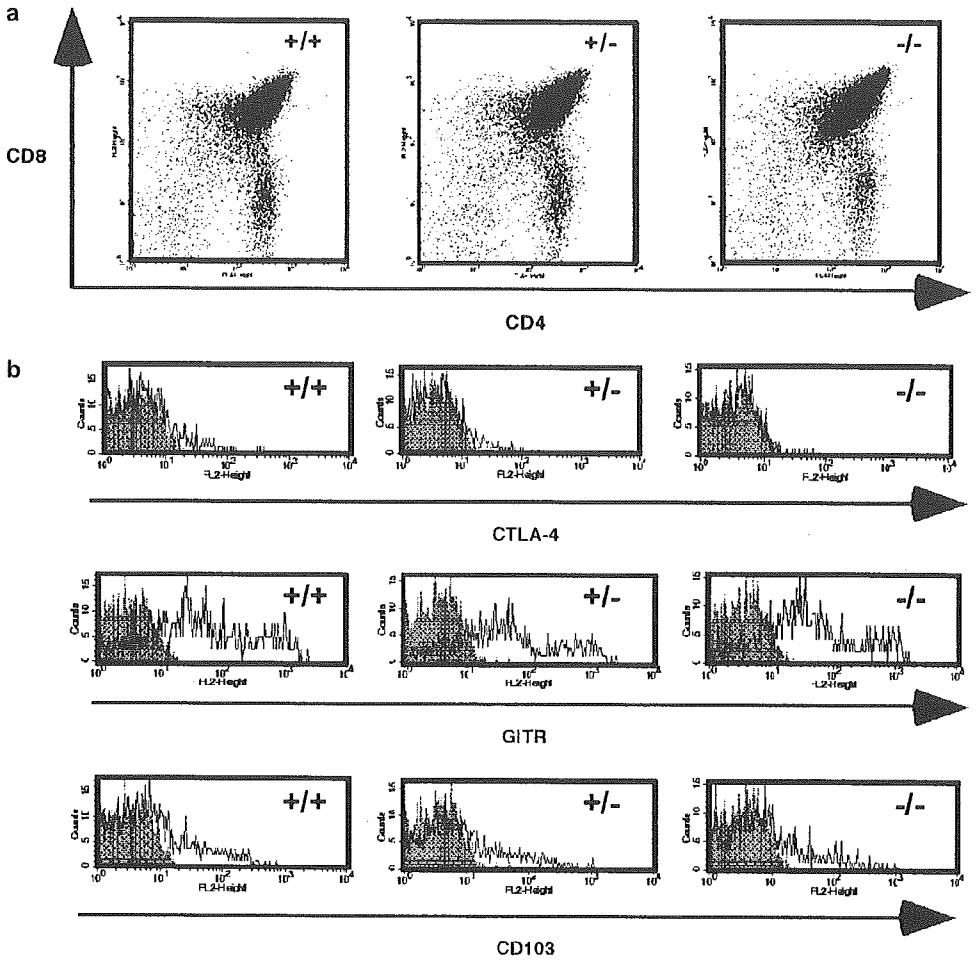
a
CD8
CD4
+/+
+/-
-/-
b
CTLA-4
GITR
CD103
+/+
+/-
-/-
c
Proliferation (x10-3 cpm)
+/+25+
+/-25+
-/-25+
adult25+
adult25-
d
Proliferation (x10-3 cpm)
Added cell counts (x10-3)/ well

respectively (data not shown). TCR stimulation induced CD25 expression on $CD25^-$ T cells, although these cells did not show suppressive activity (7). Thus, Treg and activated T cells could not be discriminated in peripheral T cells from adult CTLA-$4^{-/-}$ mice. We therefore characterized Treg in thymocytes from 10- to 12-day old CTLA-$4^{-/-}$ mice that have normal thymocyte subsets (Fig. 3a) (25). $CD25^+CD4SP$ cells constituted 5% of the CD4SP cells in CTLA-$4^{+/+}$, $^{+/-}$ and $^{-/-}$ genotypes (data not shown), suggesting that Treg normally developed in the thymi of these young CTLA-$4^{-/-}$ mice.

We isolated $CD25^+CD4SP$ thymocytes from 10- to 12-day-old CTLA-$4^{+/+}$ ($+/+25^+$), $^{+/-}$ ($+/-25^+$) and $^{-/-}$ ($-/-25^+$) mice by cell sorting. CTLA-4 was expressed on $+/+25^+$ and $+/-25^+$ but not on $-/-25^+$, whereas both GITR and CD103 were equally expressed on these cells (Fig. 3b). Similar to $+/+25^+$, $+/-25^+$ and peripheral Treg (adult $CD25^+$), $-/-25^+$ cells themselves did not respond to TCR stimulation (Fig. 3c). However, by mixing with adult $CD25^-$ cells as responder cells, $-/-25^+$ cells suppressed the proliferation of responder T cells in a dose-dependent manner, similar to $+/+25^+$ and $+/-25^+$ cells. In contrast, no $CD25^-CD4SP$ cells from either genotype showed such suppression (Fig. 3d).

Taken together, these results demonstrate that CTLA-4 is not essential for the *in vitro* suppressive activity of $CD25^+CD4SP$ thymocytes. The reason why the suppressive activity of $-/-25^+$ cells seems to be weaker than that of $+/-25^+$ cells may be attributed to the contaminated $CD25^-CD4SP$ thymocytes, as $CD25^-CD4SP$ cells from CTLA-$4^{-/-}$ mice were hyper-responsive to TCR stimulation compared with those from the other genotypes (data not shown). Nevertheless, it cannot be excluded that a minor population of Treg mediate the suppression in a CTLA-4-dependent manner.

Discussion

We addressed the question of whether CTLA-4 is required by Treg to exert suppressive activity by analyzing mice with over-expression and deletion of CTLA-4. Treg from both FL and TL Tg mice expressed the same level of *Foxp3* as $WT25^+$ and exhibited similar suppressive activity to $WT25^+$, indicating that the constitutive expression of CTLA-4 does not augment the suppressive activity of Treg. We obtained the answer to the question of the suppressive activity of Treg in CTLA-$4^{-/-}$ mice by utilizing $CD25^+CD4SP$ thymocytes from 10- to 12-day old CTLA-$4^{-/-}$ mice, based on the observation that none of the activated T cells invaded thymi at this stage (26). We found that $CD25^+CD4SP$ thymocytes differentiated normally in CTLA-$4^{-/-}$ thymus and could exert *in vitro* suppressive activity. These results suggest that CTLA-4 is not essential for the Treg-mediated suppression and its expression level does not affect the suppressive activity of Treg.

The analysis of *Foxp3* mRNA expression in these Tg mice demonstrated that the over-expression of CTLA-4 neither enhanced *Foxp3* mRNA expression in Treg nor induced it in non-regulatory cells. The number of peripheral Treg from FL and TL mice was reduced and *Foxp3* mRNA expression in these Treg was the same as that in WT Treg, consistent with the current idea that *Foxp3* expression developmentally determines the cell lineage of Treg. The apparently decreased number of Treg in both Tg mice may result from the inhibition of CD28-mediated co-stimulation by the expressed CTLA-4 because co-stimulation is required for the development and homeostasis of Treg.

On the other hand, our data showed that the physiological level of the CTLA-4 expression in $CD25^-$ non-Treg did not induce suppressive activity. $FL25^-$ neither expressed *Foxp3* nor mediated significant suppression in spite of the similar level of CTLA-4 expression to Treg. In contrast, $TL25^-$ expressed extremely high levels of CTLA-4 on the cell surface and exhibited as strong a suppressive activity as Treg. These results indicate that non-Treg do not acquire Treg function by constitutive expression of the physiological level of CTLA-4, whereas the excessive expression of the cell-surface CTLA-4 may induce suppression, probably by inhibiting the B7–CD28 interaction.

It has been shown that Treg modulate tryptophan metabolism in dendritic cells to mediate suppressive effects in a CTLA-4-dependent fashion (26). Therefore, Treg or even CTLA-4-expressing non-Treg may induce such a function. However, because we used splenocytes as APC, the *in vitro* suppression in our results may not be relevant to this regulation.

The survival of CTLA-4-Ig-treated CTLA-$4^{-/-}$ mice and mice deficient in B7 or CD28 reveals that co-stimulation through the B7–CD28 pathway is essential for the development of lymphoproliferative disorder in CTLA-$4^{-/-}$ mice (1, 3, 27). These results suggest that the blockade of B7 by CTLA-4 expressed on $CD25^-$ cells may inhibit the expansion of self-reactive T cells as an additional mechanism for preventing the development of autoimmune disease. Both Tg mice, however, survived as long as normal mice (24), suggesting that such a small number of Treg are sufficient to prevent the development of autoimmune disease and/or that CTLA-4 expression in autoreactive T cells may prevent their proliferation.

In spite of the normal development of Treg with suppressive activity in the thymus, CTLA-$4^{-/-}$ mice developed a fatal lymphoproliferative disease, despite the presence of such suppressive $CD25^+CD4SP$ cells, suggesting that CTLA-4 deficiency might impair not the development but the maintenance of Treg in the periphery. This suggestion is supported by the fact that CTLA-$4^{-/-}$ *Foxp3* Tg mice have increased numbers of $CD25^+CD4^+$ T cells and survive longer than CTLA-$4^{-/-}$ mice (28). Whereas the homeostasis of Treg depends on MHC (29) and CD28 (30), its dependence on CTLA-4 remains unknown. The adoptive transfer of splenocytes from CTLA-$4^{-/-}$ mice produces lymphoproliferative disorder, and the co-transfer of WT splenocytes prevents disease development (31). $CD25^+$ T cells isolated from peripheral T cells of adult CTLA-$4^{-/-}$ mice were shown to exhibit weak suppressive activity, and normal Treg suppressed the proliferation of $CD25^-$ T cells from CTLA-$4^{-/-}$ mice *in vitro* (14). These results suggest that a fatal lymphoproliferative disorder in CTLA-$4^{-/-}$ mice may result from a deficiency or a functional impairment of Treg in the periphery. In addition, the intrinsic activation of autoreactive $CD25^-$ T cells and the maintenance of T cell homeostasis were also impaired due to the lack of CTLA-4-mediated inhibitory signaling because CTLA-4 can induce ligand-independent inhibitory function (1).

In summary, CTLA-$4^{-/-}$ mice have normal Treg in their thymi and CTLA-4 Tg mice have a small number of Treg, indicating

that CTLA-4 is dispensable for Treg development in the thymus but plays a role in regulating the number of Treg in the periphery. For peripheral $CD25^-$ T cells, CTLA-4 may inhibit the expansion of autoreactive $CD25^-$ T cells and contribute to the maintenance of T cell homeostasis. Further analysis of the mechanism of CTLA-4-mediated regulation of Treg homeostasis may lead to the elucidation of Treg-mediated suppression of autoimmunity.

Acknowledgements

We thank H. Arase for discussion, M. Sakuma and R. Shiina for experimental assistance, and H. Yamaguchi for secretarial assistance. This work was supported by grants from the Ministry of Education, Culture, Sports, Science, and Technology, Japan.

Abbreviations

APC	antigen-presenting cells
CTLA-4	cytotoxic T lymphocyte antigen-4
FL	full length
Foxp3	*forkhead box P3*
GITR	glucocorticoid-induced tumor necrosis factor receptor
SA	streptavidin
SP	single positive
Tg	transgenic
TL	tail-less
Treg	regulatory T cells
WT	wild type

References

1 Salomon, B. and Bluestone, J. A. 2001. Complexities of CD28/B7: CTLA-4 costimulatory pathways in autoimmunity and transplantation. *Annu. Rev. Immunol.* 19:225.
2 Saito, T. and Yamasaki, S. 2003. Negative feedback of T cell activation through inhibitory adapters and costimulatory receptors. *Immunol. Rev.* 192:143.
3 Chambers, C. A., Kuhns, M. S., Egen, J. G. and Allison, J. P. 2001. CTLA-4-mediated inhibition in regulation of T cell responses: mechanisms and manipulation in tumor immunotherapy. *Annu. Rev. Immunol.* 19:565.
4 Waterhouse, P., Penninger, J. M., Timms, E. *et al.* 1995. Lymphoproliferative disorders with early lethality in mice deficient in Ctla-4. *Science* 270:985.
5 Sakaguchi, S., Sakaguchi, N., Asano, M., Itoh, M. and Toda, M. 1995. Immunologic self-tolerance maintained by activated T cells expressing IL-2 receptor alpha-chains (CD25). Breakdown of a single mechanism of self-tolerance causes various autoimmune diseases. *J. Immunol.* 155:1151.
6 Suri-Payer, E., Amar, A. Z., Thornton, A. M. and Shevach, E. M. 1998. CD4+CD25+ T cells inhibit both the induction and effector function of autoreactive T cells and represent a unique lineage of immunoregulatory cells. *J. Immunol.* 160:1212.
7 Thornton, A. M. and Shevach, E. M. 1998. CD4+CD25+ immunoregulatory T cells suppress polyclonal T cell activation *in vitro* by inhibiting interleukin 2 production. *J. Exp. Med.* 188:287.
8 Takahashi, T., Kuniyasu, Y., Toda, M. *et al.* 1998. Immunologic self-tolerance maintained by CD25+CD4+ naturally anergic and suppressive T cells: induction of autoimmune disease by breaking their anergic/suppressive state. *Int. Immunol.* 10:1969.
9 Piccirillo, C. A., Letterio, J. J., Thornton, A. M. *et al.* 2002. CD4(+)CD25(+) regulatory T cells can mediate suppressor function in the absence of transforming growth factor beta1 production and responsiveness. *J. Exp. Med.* 196:237.
10 Jordan, M. S., Boesteanu, A., Reed, A. J. *et al.* 2001. Thymic selection of CD4+CD25+ regulatory T cells induced by an agonist self-peptide. *Nat. Immunol.* 2:301.
11 Papiernik, M., de Moraes, M. L., Pontoux, C., Vasseur, F. and Penit, C. 1998. Regulatory CD4 T cells: expression of IL-2R alpha chain, resistance to clonal deletion and IL-2 dependency. *Int. Immunol.* 10:371.
12 Asano, M., Toda, M., Sakaguchi, N. and Sakaguchi, S. 1996. Autoimmune disease as a consequence of developmental abnormality of a T cell subpopulation. *J. Exp. Med.* 184:387.
13 Itoh, M., Takahashi, T., Sakaguchi, N. *et al.* 1999. Thymus and autoimmunity: production of CD25+CD4+ naturally anergic and suppressive T cells as a key function of the thymus in maintaining immunologic self-tolerance. *J. Immunol.* 162:5317.
14 Takahashi, T., Tagami, T., Yamazaki, S. *et al.* 2000. Immunologic self-tolerance maintained by CD25(+)CD4(+) regulatory T cells constitutively expressing cytotoxic T lymphocyte-associated antigen 4. *J. Exp. Med.* 192:303.
15 Shimizu, J., Yamazaki, S., Takahashi, T., Ishida, Y. and Sakaguchi, S. 2002. Stimulation of CD25(+)CD4(+) regulatory T cells through GITR breaks immunological self-tolerance. *Nat. Immunol.* 3:135.
16 McHugh, R. S., Whitters, M. J., Piccirillo, C. A. *et al.* 2002. CD4(+)CD25(+) immunoregulatory T cells: gene expression analysis reveals a functional role for the glucocorticoid-induced TNF receptor. *Immunity* 16:311.
17 Read, S., Malmstrom, V. and Powrie, F. 2000. Cytotoxic T lymphocyte-associated antigen 4 plays an essential role in the function of CD25(+)CD4(+) regulatory cells that control intestinal inflammation. *J. Exp. Med.* 192:215.
18 Chai, J. G., Tsang, J. Y., Lechler, R., Simpson, E., Dyson, J. and Scott, D. 2002. CD4+CD25+ T cells as immunoregulatory T cells *in vitro*. *Eur. J. Immunol.* 32:2365.
19 Brunkow, M. E., Jeffery, E. W., Hjerrild, K. A. *et al.* 2001. Disruption of a new forkhead/winged-helix protein, scurfin, results in the fatal lymphoproliferative disorder of the scurfy mouse. *Nat. Genet.* 27:68.
20 Wildin, R. S., Ramsdell, F., Peake, J. *et al.* 2001. X-linked neonatal diabetes mellitus, enteropathy and endocrinopathy syndrome is the human equivalent of mouse scurfy. *Nat. Genet.* 27:18.
21 Hori, S., Nomura, T. and Sakaguchi, S. 2003. Control of regulatory T cell development by the transcription factor Foxp3. *Science* 299:1057.
22 Zhumabekov, T., Corbella, P., Tolaini, M. and Kioussis, D. 1995. Improved version of a human CD2 minigene based vector for T cell-specific expression in transgenic mice. *J. Immunol. Methods* 185:133.
23 Nakaseko, C., Miyatake, S., Iida, T. *et al.* 1999. Cytotoxic T lymphocyte antigen 4 (CTLA-4) engagement delivers an inhibitory signal through the membrane-proximal region in the absence of the tyrosine motif in the cytoplasmic tail. *J. Exp. Med.* 190:765.
24 Takahashi, S., Kataoka, H., Hara, S. *et al.* 2005. *In vivo* overexpression of CTLA-4 suppresses lymphoproliferative disorders and thymic negative selection. *Eur. J. Immunol.* 35:399.
25 Chambers, C. A., Cado, D., Truong, T. and Allison, J. P. 1997. Thymocyte development is normal in CTLA-4-deficient mice. *Proc. Natl Acad. Sci. USA* 94:9296.
26 Fallarino, F., Grohmann, U., Hwang, K. W. *et al.* 2003. Modulation of tryptophan catabolism by regulatory T cells. *Nat. Immunol.* 4:1206.
27 Chambers, C. A., Sullivan, T. J. and Allison, J. P. 1997. Lymphoproliferation in CTLA-4-deficient mice is mediated by costimulation-dependent activation of CD4+ T cells. *Immunity* 7:885.
28 Khattri, R., Cox, T., Yasayko, S. A. and Ramsdell, F. 2003. An essential role for scurfin in CD4+CD25+ T regulatory cells. *Nat. Immunol.* 4:337.
29 Gavin, M. A., Clarke, S. R., Negrou, E., Gallegos, A. and Rudensky, A. 2002. Homeostasis and anergy of CD4(+)CD25(+) suppressor T cells *in vivo*. *Nat. Immunol.* 3:33.
30 Tang, Q., Henriksen, K. J., Boden, E. K. *et al.* 2003. Cutting edge: CD28 controls peripheral homeostasis of CD4+CD25+ regulatory T cells. *J. Immunol.* 171:3348.
31 Tivol, E. A. and Gorski, J. 2002. Re-establishing peripheral tolerance in the absence of CTLA-4: complementation by wild-type T cells points to an indirect role for CTLA-4. *J. Immunol.* 169:1852.

THE JOURNAL OF IMMUNOLOGY

CUTTING EDGE

Cutting Edge: Fas Ligand (CD178) Cytoplasmic Tail Is a Positive Regulator of Fas Ligand-Mediated Cytotoxicity[1]

Satoshi Jodo,[2] Vyankatesh J. Pidiyar,[2†] Sheng Xiao,[†] Akira Furusaki,[*] Rahul Sharma,[†] Takao Koike,[*] and Shyr-Te Ju[3†]*

The cytotoxic function of CD178 (Fas ligand (FasL)) is critical to the maintenance of peripheral tolerance and immune-mediated tissue pathology. The active site of FasL resides at the FasL extracellular region ($FasL_{Ext}$) and it functions through binding/cross-linking Fas receptor on target cells. In this study, we report that $FasL_{Ext}$-mediated cytotoxicity is regulated by the FasL cytoplasmic tail ($FasL_{Cyt}$). Deleting the N-terminal 2–70 aa (Δ70) or N-terminal 2–33 aa (Δ33) reduced the cytotoxic strength as much as 30- to 100-fold. By contrast, change in the cytotoxic strength was not observed with FasL deleted of the proline-rich domains (45–74 aa, ΔPRD) in the $FasL_{Cyt}$. Our study identifies a novel function of $FasL_{Cyt}$ and demonstrates that $FasL_{2-33}$, a sequence unique to FasL, is critically required for the optimal expression of $FasL_{Ext}$-mediated cytotoxicity. The Journal of Immunology, 2005, 174: 4470–4474.

Fas (CD95) is a type I transmembrane protein expressed by many nucleated cells (1). The physiological ligand for Fas (FasL,[4] or CD178) is a type II transmembrane protein expressed by activated T cells and non-T cells under a variety of conditions (2, 3). The extracellular domain of FasL ($FasL_{Ext}$) has the ability to bind Fas of target cells. Cross-linking of Fas induces target cells to undergo apoptosis (4). The FasL-mediated apoptosis pathway has been implicated in peripheral tolerance (1, 2), tissue pathology (5, 6), and maintenance of the immune privileged sites (7).

FasL expression is regulated at the transcriptional, translational, and posttranslational levels. An effective way to down-regulate FasL expression is by shedding that generates soluble FasL (sFasL). Shed sFasL exhibits weak cytotoxicity and excess sFasL inhibits FasL-based, cell-mediated cytotoxicity (8). FasL is also released from cells in the form of vesicles (FasL vesicle preparation (VP)). FasL VP display full-length FasL and express strong cytotoxicity (9, 10). The physiological significance of FasL VP remains unknown.

Among TNF family members, FasL possesses a distinctive cytoplasmic tail ($FasL_{Cyt}$) of 80 aa. The sequence of $FasL_{Cyt}$ is highly conserved among species, suggesting it may have specific functions (11–14). Here, we report a novel function of $FasL_{Cyt}$. We found that $FasL_{Cyt}$ is critically required for the full expression of FasL-mediated cytotoxicity, a function associated with $FasL_{Ext}$. Compared with $FasL_{Cyt}$ deletion mutants, $FasL_{Cyt}$ enhances cytotoxicity by as much as 30- to 100-fold. In addition, we identified $FasL_{2-33}$, a unique sequence not found in other proteins, as the positive regulator of FasL-mediated cytotoxicity. Our study demonstrates a novel regulatory function of $FasL_{2-33}$ for an effector mechanism that is critically involved in various important aspects of the immune system.

Materials and Methods

Cell lines and reagents

Neuro-2a (mouse neuroblastoma), NIH-3T3 (mouse fibroblast), and COS-7 (monkey kidney fibroblast) were obtained from American Type Culture Collection (ATCC). G247.4, NOK-1 mAb, and PE-conjugated streptavidin were obtained from BD Biosciences. All restriction endonucleases were obtained from New England Biolabs. The prokaryotic expression vector pBlueScript II KS was obtained from Stratagene. The human FasL cDNA construct and the mammalian expression vector BCMGSneo were kindly provided by Dr. S. Nagata of Osaka University Medical Center (Osaka, Japan) (11).

Construction of FasL deletion mutants

The full-length human FasL cDNA cloned in pBlueScript II KS was used to generate deletion mutants by PCR using different 5′ primers and the same 3′ primer (Integrated DNA Technologies). All 5′ primers used contain the translation start sequence ATG that codes for methionine. therefore, deletion begins with amino acid residue 2 of FasL. The sequences of the 5′ primers are: 5′-ATGACCTCTGTGCCCAGAAGGCC-3′ (for Δ33 in which $FasL_{2-33}$ is deleted), 5′-ATGCTGAAGAAGAGAGGGAACCACAGC-3′ (for Δ70 in which $FasL_{2-70}$ is deleted), 5′-ATGCAGCTCTTCCACCTACAGAAG GAGC-3′ (for Δ102 in which $FasL_{2-102}$ is deleted) and 5′-GGCCTGGT CAAAGGAGGGGGAACCACAGCACAGGC-3′ (for ΔPRD (proline-rich domain deletion mutant) in which $FasL_{45-74}$ is deleted). We used Δ102 FasL together with BCMGSneo (vector control (Vc)) in every transfection experiment to control any unforeseen effect of our recombinant engineering process. The sequence of the 3′ primer is 5′-GTAAAACGACGGCCAGTGAGCG-3′ of the pBlueScript II KS. The PCR products were subcloned into pBlueScript II KS. The inserts were excised with *Not*I and *Xho*I and cloned into the BCMGSneo vector. The gene sequence of each construct was confirmed by DNA sequencing.

[*]Department of Medicine II, Hokkaido University Graduate School of Medicine, Sapporo, Japan; and [†]Division of Rheumatology and Immunology, Department of Internal Medicine, University of Virginia, Charlottesville, VA 22908

Received for publication October 13, 2004. Accepted for publication February 8, 2005.

The costs of publication of this article were defrayed in part by the payment of page charges. This article must therefore be hereby marked *advertisement* in accordance with 18 U.S.C. Section 1734 solely to indicate this fact.

[1] This work was supported in part by National Institutes of Health Grant AI36938.

[2] S.J. and V.J.P. contributed equally to this work.

[3] Address correspondence and reprint requests to Dr. Shyr-Te Ju, Division of Rheumatology and Immunology, Department of Internal Medicine, University of Virginia, Charlottesville, VA 22908-0412. E-mail address: sj8r@virginia.edu

[4] Abbreviations used in this paper: FasL, Fas ligand; $FasL_{Ext}$, FasL extracellular domain; sFasL, soluble FasL; VP, vesicle preparation; $FasL_{Cyt}$, FasL cytoplasmic tail; PRD, proline-rich domain; Vc, vector control; WT, wild type.

0022-1767/05/$02.00

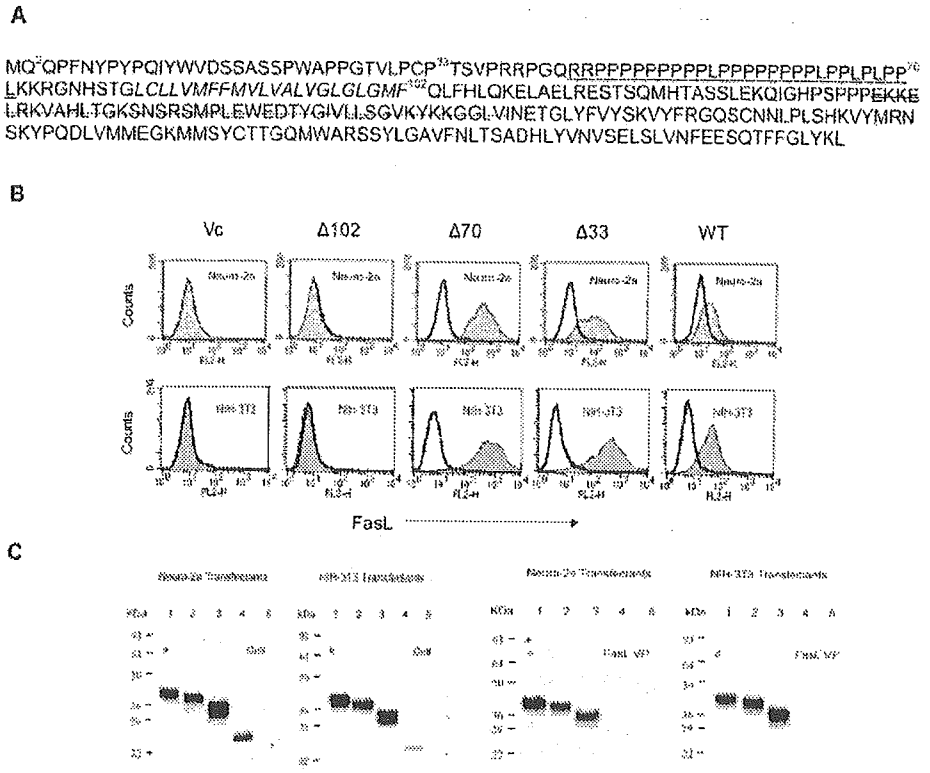

FIGURE 1. Cell surface expression of FasL by various transfectants. The WT human FasL sequence was shown in *A*. The amino acid positions 2, 33, 70, and 102 were marked to indicate the sequence deleted for Δ33 (2–33), Δ70 (2–70), and Δ102 (2–102) FasL mutants. PRD is underlined. The transmembrane domain is italicized. The strike-through sequence represents the trimerization motif. *B*, Various Neuro-2a transfectants (*upper panels*) and NIH-3T3 transfectants (*lower panels*) were stained with biotin-conjugated NOK-1 mAb (shaded area) or isotype control (open area), followed by FITC-conjugated streptavidin and analyzed with a flow cytometer. Data presented is representative of three separate experiments. *C*, Western blot analysis of FasL of various transfectants (*a* and *b*) and their FasL VP (*c* and *d*) of Neuro-2a and NIH-3T3 series. *Lanes 1–5* are samples from WT, Δ33, Δ70, Δ102, and Vc transfectants, respectively. Molecular mass markers are shown on the *left side* of each panel.

Transfection

The derivation, characterization, and culture condition for maintenance of transfectants of various cell lines have been described (15).

Flow cytometric analysis

Cells (0.5×10^6) were suspended in 0.1 ml of PBS containing 0.2% BSA and 1 μg of biotinylated NOK-1 or biotinylated control isotype. Binding reaction was conducted at 4°C for 30 min with gentle mixing periodically. Afterward, cells were washed twice with cold PBS. Bound Abs were measured by incubating with 0.5 μg of FITC-conjugated streptavidin for 30 min at 4°C. Cells were washed twice with cold PBS and then analyzed using FACScan (BD Biosciences) equipped with CellQuest software. At least 2×10^4 stained cells in the gated area were selected with each sample.

Preparation of sFasL and FasL VP

Cells at ~80% confluence were maintained in 150 mm × 25 mm petri dishes in 25 ml of culture medium for 48 h. FasL VP and sFasL were prepared as previously described (9, 10).

Table I. *FasL protein levels in various compartments of transfectant culture*[a]

	WT	Δ33	Δ70	Δ102[b]	Vc[b]
Neuro-2a[c]					
Cell lysate	3	19	89	<0.01	<0.01
FasL VP	17	14	50	<0.02	<0.02
sFasL	9	15	10	<0.2	<0.2
NIH-3T3[c]					
Cell lysate	8	65	72	<0.01	<0.01
FasL VP	31	44	54	<0.02	<0.02
sFasL	46	139	132	<0.2	<0.2

[a] FasL in samples was determined by ELISA. Data presented are representative of three separate experiments.

[b] The numbers indicate the limits of FasL detection, which depend on sample volumes used in the assay.

[c] The numbers indicate FasL total amounts in picomoles in samples. See *Materials and Methods* for sample preparation.

Quantification of FasL

The amounts of FasL in cell extract, FasL VP, and sFasL of all transfectants were determined using the $FasL_{Exc}$-specific ELISA kit (Oncogene) as previously described (10). A standard curve using recombinant sFasL provided with the kit is included in every individual assay.

Western blot analysis

Western blot analysis was conducted as previously described (9). Protein concentrations loaded were 0.1–5 μg. For samples lacking detectable FasL, 5 μg of total protein was loaded. FasL was detected using $FasL_{Exc}$-reactive G247.4 mAb followed by anti-mouse IgG-HRP (Sigma-Aldrich). Specific bands were developed using ECL (Amersham).

Cytotoxicity assay

A cytotoxicity assay was conducted as previously described using ^{51}Cr-labeled, A20 B lymphoma cells or Jurkat T lymphoma cells as targets (10). Various amounts of effector were incubated with 2×10^4 target cells for 4–8 h at 37°C in a 10% CO_2 incubator. At the end of incubation, cell-free supernatants were collected and counted with a gamma-counter (LKB). Cytotoxicity, expressed as percent-specific Cr release, was calculated by the formula: 100 × (experimental release − background release)/(total release − background release). Background release was determined by culturing target cells with medium. Total release was determined by lysing target cells with 2% Triton X-100. Experiments were conducted in duplicate and repeated at least twice.

Results and Discussion

$FasL_{Cyt}$ regulates FasL expression level

We prepared a series of FasL deletion mutant expression constructs and used them to transfect Neuro-2a and NIH-3T3 cells (Fig. 1*A*). G418-resistant transfectants were selected. We used flow cytometry to determine the cell surface expression of FasL (Fig. 1*B*). In both series of transfectants, wild-type (WT) FasL transfectants stained positive but a significantly stronger staining was observed with Δ33 and Δ70 FasL transfectants. Cell surface FasL expression was not observed with Δ102 FasL or Vc transfectants.

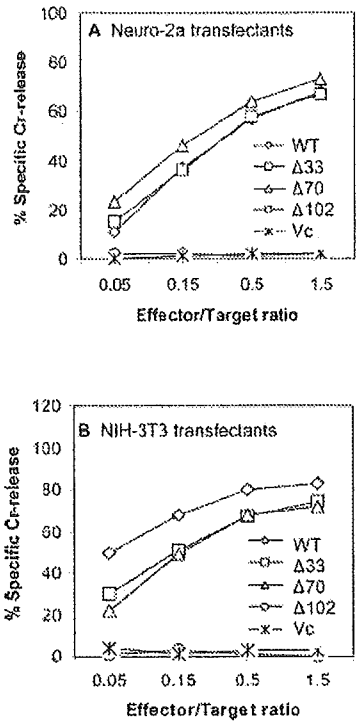

FIGURE 2. FasL-mediated cytotoxicity does not correlate with FasL membrane expression levels of transfectants. Cell-mediated cytotoxicity was conducted with various transfectants of Neuro-2a (*A*) and NIH-3T3 (*B*) series. Transfectants were cultured with ^{51}Cr-labeled Jurkat cells at various E:T ratios. The percent-specific Cr release was determined after 4 h of incubation.

We used FasL-specific ELISA to determine the total FasL levels in transfectants. Under the specific condition, WT transfectants of NIH-3T3 and Neuro-2a cell lines expressed 8 and 3 picomoles of FasL, respectively. A 6- to 30-fold increase in FasL level was observed for Δ33 FasL and Δ70 FasL transfectants. No FasL was detected in Δ102 FasL or Vc transfectants. Thus, the total FasL levels in transfectants correlated with their cell surface expression. In contrast, FasL levels in FasL VP and sFasL preparations did not correlate with the total FasL levels of transfectants (Table I). We have recently reported that the increase in FasL expression in Δ33 and Δ70 FasL transfectants is the result of an increase in the FasL translation rate (15).

We validated the size of FasL deletion mutants by Western blot analysis (Fig. 1*C*). WT, Δ33, and Δ70 FasL transfectants expressed the recombinant proteins of the predicted sizes (Fig. 1, *A* and *B*). A small size and faintly stained band was observed with the Δ102 FasL transfectant. No band was observed with Vc transfectants. FasL of predicted sizes were also observed with FasL VP prepared from the corresponding WT, Δ33, and Δ70 FasL transfectants. No band was observed with vesicles prepared from Δ102 FasL and Vc transfectants (Fig. 1*C*).

Both WT and $FasL_{Cyt}$ deletion mutants express FasL-mediated cytotoxicity

We tested these transfectants for cell-mediated cytotoxicity against the ^{51}Cr-labeled Jurkat target (Fig. 2). Cytotoxicity was not detected with Δ102 FasL and Vc transfectants. Transfectants expressing cell surface FasL displayed a dose-dependent killing based on various E:T ratios. Interestingly, the cytotoxic strength of WT FasL transfectants was comparable to that of Δ33 or Δ70 FasL transfectants despite the fact that the latter transfectants expressed significantly more FasL.

We also determined the cytotoxic strength based on the total FasL amount of transfectant using ^{51}Cr-labeled A20 B lymphoma cells as target (Fig. 3, *A* and *B*). For both series of transfectants, the cytotoxic strength of WT FasL was 10- to 30-fold stronger than that of Δ33 or Δ70 FasL transfectants. This dramatic difference is surprising because the cytotoxicity is dependent on cross-linking Fas receptors on target cells by $FasL_{Ext}$. The data therefore strongly suggest that $FasL_{Cyt}$ regulates $FasL_{Ext}$-mediated cytotoxicity across a membrane barrier. This difference in the strength of cell-mediated killing could be intrinsic to $FasL_{Cyt}$ or due to the cellular environment of FasL transfectants, or both.

Evidence from FasL VP

To firmly establish that $FasL_{Cyt}$ regulates FasL-mediated cytotoxicity, we determined the cytotoxic strength of FasL VP prepared from transfectants (Fig. 3, *C* and *D*). FasL VP is presumably a minimum subcellular component capable of expressing functional FasL transmembrane protein. It is free from sFasL. Its cytotoxicity, unlike transfectants, does not depend on protein synthesis (10). Using the same amount of FasL, FasL VP derived from WT FasL transfectants of Neuro-2a or NIH-3T3 delivered 10- to 30-fold stronger cytotoxicity than the FasL VP

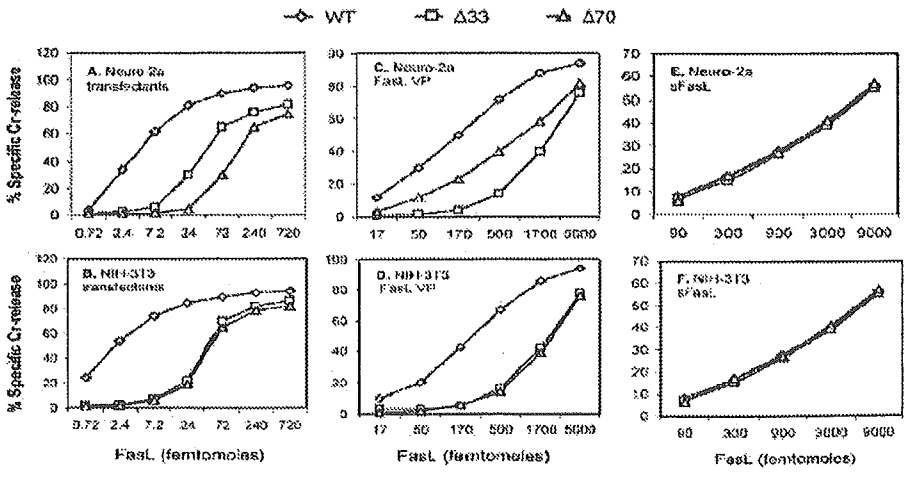

FIGURE 3. Comparison of cytotoxicity mediated by cells, FasL VP, and sFasL of various transfectants. Cells (*A* and *B*), FasL VP (*C* and *D*), and sFasL (*E* and *F*) of Neuro-2a (*A*, *C*, and *E*) and NIH-3T3 series (*B*, *D*, and *F*) were incubated with ^{51}Cr-labeled A20 target cells at various molar concentrations of FasL for 4 (cells and FasL VP) or 8 h (sFasL). Afterward, supernatants were removed and counted. The cytotoxicity data presented is representative of three experiments.

derived from Δ33 or Δ70 FasL transfectants. By contrast, the sFasL derived from these transfectants, either from Neuro-2a series (Fig. 3*E*) or from NIH-3T3 series (Fig. 3*F*), displayed nearly identical cytotoxicity. The data suggest that $FasL_{2-33}$ is important for the optimal expression of FasL-mediated cytotoxicity.

$FasL_{2-33}$ but not $FasL_{PRD}$ is required for the optimal expression of FasL-mediated cytotoxicity

$FasL_{Cyt}$ contains PRD that may interact with certain cellular proteins (12). To determine whether $FasL_{PRD}$ plays a role in FasL-mediated cytotoxicity, we generated PRD-deleted (ΔPRD) FasL transfectants from Neuro-2a and COS-7 cell lines. In contrast to Δ33 and Δ70 FasL transfectants, FasL expression was not increased in ΔPRD transfectants (data not shown). We prepared FasL VP from these transfectants and determined their cytotoxic strength (Fig. 4). For both Neuro-2a and COS-7 transfectants, the cytotoxic strength of ΔPRD FasL VP was comparable to WT FasL VP. As controls, FasL VP prepared from Δ33 FasL Neuro-2a transfectant and Δ70 FasL COS-7 transfectant displayed cytotoxicity 30- to 100-fold less than WT FasL VP. The data indicate that $FasL_{PRD}$ is not required for the optimal expression of FasL-mediated cytotoxicity. Taken together, the critical role of $FasL_{2-33}$ is demonstrated both by its deletion (as in Δ33 FasL and Δ70 FasL) that resulted in losing the $FasL_{Ext}$ cytotoxic strength and by its presence (as in ΔPRD FasL and WT FasL) that resulted in optimal display of $FasL_{Ext}$ cytotoxicity.

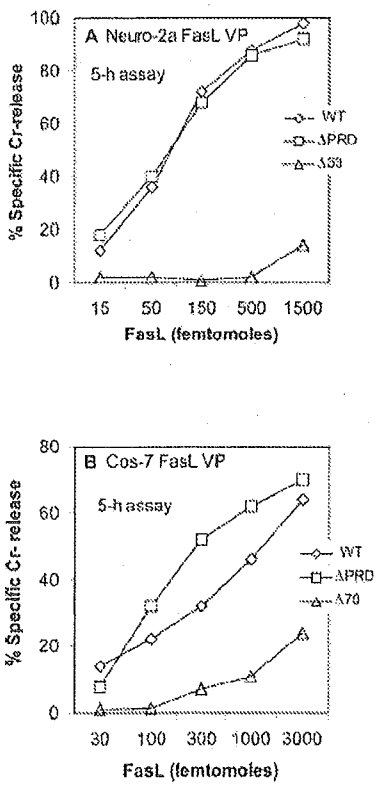

FIGURE 4. $FasL_{PRD}$ is not required for the optimal expression of FasL-mediated cytotoxicity. Samples of FasL VP were prepared from WT and ΔPRD FasL transfectants of Neuro-2a and COS-7 cell lines. FasL contents were determined using ELISA. Various amounts of FasL were compared for cytotoxic strength against ^{51}Cr-labeled A20 target. As controls, FasL VP prepared from Δ33 FasL Neuro-2a transfectant and Δ70 FasL COS-7 transfectant were analyzed in parallel. The data presented is representative of three experiments.

Our study used an artificial expression system to determine the structure and function relationship between $FasL_{Cyt}$ and $FasL_{Ext}$-mediated cytotoxicity. Deletion of $FasL_{Cyt}$ could potentially result in different localization of cell membrane FasL, change in sFasL production, faster FasL membrane movement, loss of interaction with $FasL_{Cyt}$-interacting proteins, loss of the ability to form oligomers, changes in $FasL_{Ext}$ conformation, change in phosphorylation state, etc. Additional studies are needed to determine the precise mechanism(s) and FasL-bearing vesicles offer a simple and novel system for this purpose and perhaps for other bioactive transmembrane proteins. Among these possibilities, we have ruled out the overproduction of sFasL as a mechanism for the down-regulation of cell-mediated cytotoxicity. Moreover, under the assay conditions, sFasL released were insufficient to influence the cell-mediated cytotoxicity (10). Our data further indicate that the weakened cytotoxic potential of sFasL is in part due to loss of $FasL_{Cyt}$, in addition to loss of multivalency as previously described (8). The observation that $FasL_{PRD}$ did not play a role in FasL-mediated cytotoxicity rules out the participation of potential $FasL_{PRD}$-interacting proteins such as Grb2, Grap, $p47^{phox}$, and Nck in this process (12). Moreover, no interacting protein was detected using GST-$FasL_{2-29}$ (12). These data suggest the ability to optimize FasL cytotoxicity is intrinsic to $FasL_{2-33}$. $FasL_{2-33}$ contains a DSSASSP motif that is a potential substrate for CK-I, CK-II, and GSK-3 kinases. Among them, the CK-I site (SXXS) is shared with several TNF superfamily members. Otherwise, $FasL_{2-33}$, including the Cys_{32}, a potential site for disulfide bonding and acetylation/palmitoylation, is unique among members of the TNF superfamily (⟨www.ncbi.nlm.nih.gov⟩). These properties should be helpful in determining the molecular mechanism by which the FasL-based cytotoxicity is optimized. The dramatic enhancement of cytotoxicity by $FasL_{2-33}$ may explain why FasL plays a critical role in peripheral tolerance and immune-mediated tissue damage that is dependent on cytotoxicity strength.

A regulatory role of $FasL_{Cyt}$ on $FasL_{Ext}$-mediated cytotoxicity had not been previously envisaged and our study provides the first definitive evidence supporting this novel function. Our study has significant implications with respect to regulation of membrane protein function in general and we have demonstrated this significant point in one effector function that is critically involved in peripheral tolerance, lymphocyte homeostasis, and immune-mediated tissue pathology. Our results also point out a potential complication in studies in which the cytoplasmic tail of a transmembrane protein is deleted by recombinant engineering as well as the potential use of *$FasL_{Cyt}$* and *$FasL_{2-33}$* to control the expression levels and biochemical properties of transmembrane proteins.

Acknowledgments

We thank Drs. S. M. Fu, S.-s. J. Sung, M. Brown, and T. Braciale for their critical comments and suggestions.

Disclosures

The authors have no financial conflict of interest.

References

1. Watanabe-Fukunaga, R., C. I. Brannan, N. G. Copeland, N. A. Jenkins, and S. Nagata. 1992. Lymphoproliferative disorder in mice explained by defects in Fas antigen that mediates apoptosis. *Nature 356:314.*
2. Takahashi, T., M. Tanaka, C. I. Brannan, N. A. Jenkins, N. G. Copeland, T. Suda, and S. Nagata. 1994. Generalized lymphoproliferative disease in mice, caused by a point mutation in the Fas ligand. *Cell 76:969.*
3. Bonfoco, E., P. M. Stuart, T. Brunner, T. Lin, T. S. Griffith, Y. Gao, H. Nakajima, P. A. Henkart, T. A. Ferguson, and D. R. Green. 1998. Inducible nonlymphoid expression of Fas ligand is responsible for superantigen-induced peripheral deletion of T cells. *Immunity 9:711.*
4. Rouvier, E., M.-F. Luciano, and P. Golstein. 1993. Fas involvement in Ca^{2+}-independent T cell-mediated cytotoxicity. *J. Exp. Med. 177:195.*
5. Wei, Y., K. Chen, G. C. Sharp, H. Yagita, and H. Braley-Mullen. 2001. Expression and regulation of Fas and Fas ligand on thyrocytes and infiltrating cells during induction and resolution of granulomatous experimental autoimmune thyroiditis. *J. Immunol. 167:66.*
6. Pinkoski, M. J., T. Brunner, D. R. Green, and T. Lin. 2000. Fas and Fas ligand in gut and liver. *Am. J. Physiol. 278:G354.*
7. Griffith, T. S., X. Yu, J. M. Herndon, D. R. Green, and T. A. Ferguson. 1996. CD95-induced apoptosis of lymphocytes in an immune privileged site induces immunological tolerance. *Immunity 5:7.*
8. Tanaka, M., T. Itai, M. Adachi, and S. Nagata. 1998. Down-regulation of Fas ligand by shedding. *Nat. Med. 4:31.*
9. Strehlow, D., S. Jodo, and S.-T Ju. 2000. Retroviral membrane display of apoptotic effector molecules. *Proc. Nat. Acad. Sci. USA 97:4209.*
10. Jodo, S., S. Xiao, A. Hohlbaum, D. Strehlow, A. Marshak-Rothstein, and S.-T. Ju. 2001. Apoptosis-inducing membrane vesicles: a novel agent with unique properties. *J. Biol. Chem. 276:39938.*
11. Takahashi, T., M. Tanaka, J. Inazawa, T. Abe, T. Suda, and S. Nagata. 1994. Human Fas ligand: gene structure, chromosomal location and species specificity. *Int. Immunol. 6:1567.*
12. Ghadimi, M. P., Sanzenbacher, R. Thiede, B. Wenzel, J. Jing, Q. Plomann, M. Borkhard, A. D. Kabelitz, and O. Janssen. 2002. Identification of interaction partners of the cytosolic polyproline region of CD95 ligand (CD178). *FEBS Lett. 519:50.*
13. Suzuki, I., and P. J. Fink. 1998. Maximal proliferation of cytotoxic T lymphocytes requires reverse signaling through Fas ligand. *J. Exp. Med. 187:123.*
14. Blott, E. J., G. Bossi, R. Clark, M. Zvelebil, and G. M. Griffiths. 2001. Fas ligand is targeted to secretory lysosomes via a proline-rich domain in its cytoplasmic tail. *J. Cell Sci. 114:2405.*
15. Xiao, S., U. S. Deshmukh, S. Jodo, T. Koike, R. Sharma, R. Furusaki, S-s. J. Sung, and S-T. Ju. 2004. Novel negative regulator of expression in Fas ligand (CD178) cytoplasmic tail: evidence for translational regulation and against FasL retention in secretory lysosomes. *J. Immunol. 173:5095.*

Pkd1 regulates immortalized proliferation of renal tubular epithelial cells through p53 induction and JNK activation

Saori Nishio,[1,2] Masahiko Hatano,[2] Michio Nagata,[3] Shigeo Horie,[4] Takao Koike,[1] Takeshi Tokuhisa,[2] and Toshio Mochizuki[1]

[1]Department of Medicine II, Hokkaido University Graduate School of Medicine, Sapporo, Japan. [2]Department of Developmental Genetics (H2), Graduate School of Medicine, Chiba University, Chiba, Japan. [3]Department of Pathology, Institute of Basic Medical Sciences, University of Tsukuba, Tsukuba, Japan. [4]Department of Urology, Teikyo University School of Medicine, Tokyo, Japan.

Autosomal dominant polycystic kidney disease (ADPKD) is the most common human monogenic genetic disorder and is characterized by progressive bilateral renal cysts and the development of renal insufficiency. The cystogenesis of ADPKD is believed to be a monoclonal proliferation of PKD-deficient ($PKD^{-/-}$) renal tubular epithelial cells. To define the function of *Pkd1*, we generated chimeric mice by aggregation of $Pkd1^{-/-}$ ES cells and $Pkd1^{+/+}$ morulae from ROSA26 mice. As occurs in humans with ADPKD, these mice developed cysts in the kidney, liver, and pancreas. Surprisingly, the cyst epithelia of the kidney were composed of both $Pkd1^{-/-}$ and $Pkd1^{+/+}$ renal tubular epithelial cells in the early stages of cystogenesis. $Pkd1^{-/-}$ cyst epithelial cells changed in shape from cuboidal to flat and replaced $Pkd1^{+/+}$ cyst epithelial cells lost by JNK-mediated apoptosis in intermediate stages. In late-stage cysts, $Pkd1^{-/-}$ cells continued immortalized proliferation with downregulation of p53. These results provide a novel understanding of the cystogenesis of ADPKD patients. Furthermore, immortalized proliferation without induction of p53 was frequently observed in 3T3-type culture of mouse embryonic fibroblasts from $Pkd1^{-/-}$ mice. Thus, *Pkd1* plays a role in preventing immortalized proliferation of renal tubular epithelial cells through the induction of p53 and activation of JNK.

Introduction

Autosomal dominant polycystic kidney disease (ADPKD) is the most common human monogenic genetic disorder and is characterized by progressive bilateral renal enlargement with numerous cysts and fibrosis in the renal parenchyma. It is often accompanied by extra-renal manifestations, such as hypertension, intracranial aneurysms, and hepatic and pancreatic cysts (1). The disease is progressive, and many patients develop renal insufficiency in the fifth and sixth decades of life. Cystogenesis has been studied by microdissection of ADPKD kidneys. The initial event in cyst formation is believed to be the dilatation and "out-pocketing" of tubules. The cysts arise from any segment of one nephron and maintain continuity with the "parental" nephron (2). Fully developed cysts are apparently isolated from the "parental" nephron and expand through the accumulation of cyst fluid (3).

The *PKD1* gene (encoding polycystin-1) (4) and the *PKD2* gene (encoding polycystin-2) (5) have been identified by positional cloning as being the genes responsible for ADPKD. Loss of heterozygosity or second somatic mutations at the *PKD1* or *PKD2* loci have been reported in cystic epithelia from ADPKD patients (6–10). Several lines of mice in which the *Pkd1* or *Pkd2* gene was targeted show similar phenotypes. Although heterozygous knockout mice develop renal and hepatic cysts later in life (after age 16 months) (11), those mice do not fully recapitulate the severity of human ADPKD. Homozygous knockout mice die in utero and develop severely polycystic kidneys (12–16). Interestingly, compound heterozygous $Pkd2^{WS25-}$ mice, which carry a unique *Pkd2* allele that is prone to genomic rearrangement leading to a null allele, develop severely polycystic kidneys during adulthood and thus resemble the ADPKD phenotypes (12). These model animals suggested that a "2-hit" mechanism at either the *PKD1* or *PKD2* gene explains the late onset of the disease as well as some of the variation in clinical symptoms (17, 18).

The molecular mechanisms of the cyst formation of Pkd-deficient ($Pkd^{-/-}$) renal tubular epithelial cells have been studied extensively. Polycystin-1 and polycystin-2 are localized in the primary cilium of renal tubular epithelial cells (19). The relationship between cystogenesis and the disruption of cilia has been reported (20, 21). Although polycystin-2 in node monocilia contributes to the development of left-right asymmetry (22), polycystin-1 and polycystin-2 in the primary cilium transduce the extracellular mechanical stimulus induced by urinary flow into increases in cytosolic Ca^{2+}, which may regulate renal tube size (19, 23).

The cyst epithelial cells of ADPKD kidneys have a high mitotic rate in vitro (24) and in vivo, as detected by immunostaining for proliferating cell nuclear antigen (PCNA) (25), c-Myc, and Ki-67 (26). Their high mitotic rate has also been supported by the following results. First, expression of growth factors such as EGF and their receptors increases in ADPKD cysts (3, 27). Second, cAMP stimulates the in vitro proliferation of ADPKD cyst epithelium and cyst growth (28, 29). Third, overexpression of the *Pkd1* gene in a cell line induced cell cycle arrest at the G0/G1 phase with upregulation of p21 through activation of the JAK-STAT pathway (30). Thus, the proliferation of a $PKD^{-/-}$ cyst epithelial cell might explain the cystogenesis of ADPKD kidneys. However, polycystin-1

Nonstandard abbreviations used: ADPKD, autosomal dominant polycystic kidney disease; DBA, *Dolichos biflorus* agglutinin; LZ, LacZ; MEF, mouse embryonic fibroblast; p-, phosphorylated; PCNA, proliferating cell nuclear antigen.

Conflict of interest: The authors have declared that no conflict of interest exists.

Citation for this article: *J. Clin. Invest.* 115:910–918 (2005). doi:10.1172/JCI200522850.

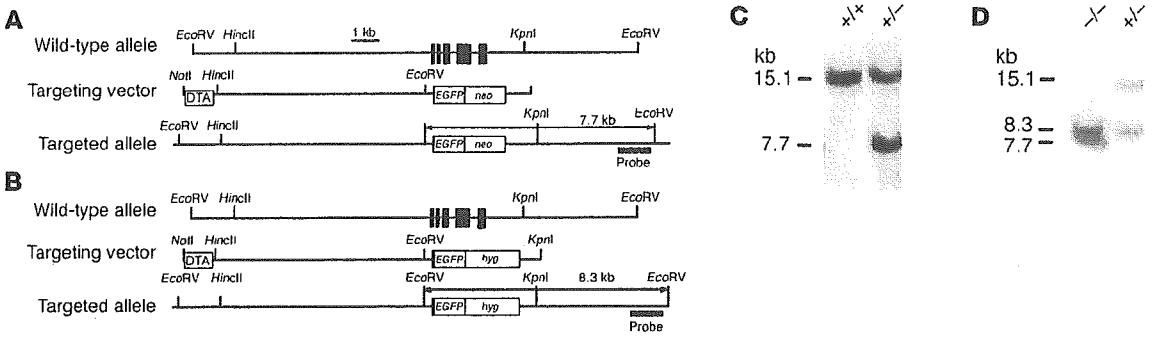

Figure 1
Generation of *Pkd1*$^{-/-}$ ES cells. (**A** and **B**) Genomic organization of 2 targeting vectors. Exons are depicted as filled boxes. The targeting vectors were designed to replace a DNA segment of exons 2–6 by a neomycin-resistance gene cassette (*neo*) (**A**) or a hygromycin-resistance gene cassette (*hyg*) (**B**). *EGFP*, gene encoding enhanced GFP. (**C** and **D**) Southern blots of genomic DNA derived from ES clones. Purified DNA was digested with *Eco*RV and bands were detected by a probe, as described in Methods. Fragments corresponding to wild-type (15.1 kb) and targeted (7.7 kb and 8.3 kb) alleles are shown. +/+, wild-type; –/–, *Pkd1*$^{-/-}$.

and polycystin-2 can be detected in some of the cyst epithelial cells of ADPKD kidneys (31–36). These results suggest a contribution of normal renal tubular epithelial cells to cystogenesis.

The cystogenesis of ADPKD kidneys cannot be fully reproduced in the kidneys of *Pkd1*$^{-/-}$ mice, because these mice die in utero and their renal tubular epithelial cells are not mosaic for *Pkd1*$^{-/-}$ and normal cells, as are ADPKD kidneys. In an attempt to establish an animal model for human ADPKD, we generated chimeric mice by an aggregation method using *Pkd1*$^{-/-}$ ES cells and normal morulae from LacZ^{+} (LZ^{+}) ROSA26 mice (37). We show here that chimeric mice with a low degree of chimerism survived for more than 1 month and had multiple cysts not only in the kidneys but also in the liver and pancreas, suggesting this may be a feasible model for human ADPKD. Surprisingly, both *Pkd1*$^{-/-}$ and wild-type (LZ^{-}) epithelial cells were involved in early cystogenesis in kidneys of the chimeric mice. We discuss here the molecular mechanisms of the cystogenesis of *Pkd1*$^{-/-}$ and *Pkd1*$^{+/+}$ renal tubular epithelial cells.

Results

Cystogenesis of Pkd1$^{-/-}$*/LZ*$^{+}$ *chimeric mice.* We generated mice carrying a mutation in the *Pkd1* gene using standard gene-targeting procedures by replacing exons 2–6 with the neomycin-resistance gene (Figure 1A). Homozygous mutant (*Pkd1*$^{-/-}$) mice died in utero with severely polycystic kidneys and cardiac abnormalities (data not shown), similar to previous descriptions (14, 15). A second targeting vector with the hygromycin-resistance gene (Figure 1B) was transfected into heterozygous (*Pkd1*$^{+/-}$) ES cells to obtain *Pkd1*$^{-/-}$ ES cells. Each gene targeting was confirmed by Southern blot (Figure 1, C and D). Then, we generated chimeric mice composed of mixtures of *Pkd1*$^{-/-}$ and wild-type cells. To monitor cells derived from *Pkd1*$^{-/-}$ ES cells in chimeric mice, we used morulae from LZ^{+} ROSA26 mice. Four independently targeted *Pkd1*$^{-/-}$ ES clones were aggregated with ROSA26 morulae to generate *Pkd1*$^{-/-}$/LZ^{+} chimeric mice.

Several *Pkd1*$^{-/-}$/LZ^{+} mice survived beyond 1 month of age, and their survival closely depended on the degree of chimerism, as estimated by coat color. When the contribution of *Pkd1*$^{-/-}$ ES cells to coat color was more than 30%, the chimeric mice either died in utero or died by P7 with severely polycystic kidneys. *Pkd1*$^{-/-}$/LZ^{+} mice with a lower contribution (less than 10%) of *Pkd1*$^{-/-}$ ES cells to their coat color survived beyond 1 month of age. Renal cysts were detected in all the *Pkd1*$^{-/-}$/LZ^{+} mice examined (n = 90). When we compared chimerism and cyst formation in P7 *Pkd1*$^{-/-}$/LZ^{+} kidneys, the incidence of cysts roughly correlated with the degree of chimerism (Figure 2, A and B). *Pkd1*$^{-/-}$/LZ^{+} kidneys were enlarged due to scattered tubular cysts observed in both the cortex and the outer medulla. These cysts occupied roughly 20–90% of the cut surface of the kidneys, in parallel with the degree of chimerism. A P60 *Pkd1*$^{-/-}$/LZ^{+} mouse had bilateral enlarged kidneys deformed by many cysts and often accompanied by hemorrhage (Figure 2C). Cut surfaces of the kidney showed little renal parenchyma (Figure 2D). This mouse also exhibited hepatic and pancreatic cysts. These pathological findings in *Pkd1*$^{-/-}$/LZ^{+} mice with low degree of chimerism were similar to those of human ADPKD.

To examine initial cyst formation in kidneys of *Pkd1*$^{-/-}$/LZ^{+} and *Pkd1*$^{-/-}$ mice, we microdissected a single nephron from the kidneys of those mice at E17.5. As shown in Figure 2E, multiple "out-pocketing" cysts were observed in all segments of the nephron from *Pkd1*$^{-/-}$/LZ^{+} mice, whereas cysts in the nephrons from *Pkd1*$^{-/-}$ mice were confined mainly to the distal tubule. Surprisingly, the cyst epithelia in chimeric mice were composed of not only *Pkd1*$^{-/-}$ cells but also LZ^{+} wild-type cells, as detected by β-gal staining (Figure 2F). Histochemical examination also showed the presence of LZ^{+} wild-type cells in the cyst epithelia of *Pkd1*$^{-/-}$/LZ^{+} kidneys (Figure 2G).

Dedifferentiation of cyst epithelial cells in Pkd1$^{-/-}$ *LZ*$^{+}$ *mice.* Cystogenesis in kidneys of *Pkd1*$^{-/-}$/LZ^{+} mice with low degree of chimerism was analyzed histologically between P1 and P30. At the early stage (P1), small cysts were numerous and their cyst epithelia were composed of many LZ^{+} cells and some *Pkd1*$^{-/-}$ cells (Figure 3A). At the late stage (P30), individual cysts were enlarged and most of the cyst epithelia were composed of *Pkd1*$^{-/-}$ cells. Similar histological findings were observed in the livers of *Pkd1*$^{-/-}$/LZ^{+} mice (data not shown). Morphological analysis of cyst epithelial cells at the early stage of cystogenesis demonstrated that many of the cyst epithelial *Pkd1*$^{-/-}$ and LZ^{+} cells were cuboidal in shape (Figure 3B). Although the shape of LZ^{+} cyst epithelial cells was still cuboidal at the intermediate stage of cystogenesis, many *Pkd1*$^{-/-}$ cyst epithelial cells changed their shape from cuboidal to flat (Figure 3C), suggesting that flat cyst epithelial cells are dedifferentiated.

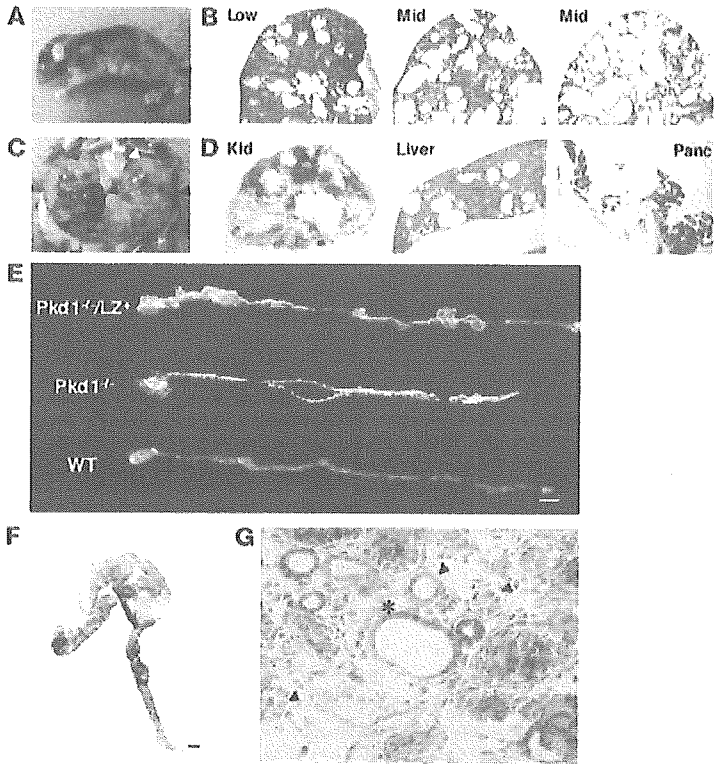

Figure 2
Pkd1$^{-/-}$/LZ^{+} mice as an animal model of human ADPKD. (**A**) Appearance of a P7 *Pkd1*$^{-/-}$/LZ^{+} mouse with an intermediate chimeric rate. The chimeric rate was estimated by coat color. (**B**) Kidneys of P7 *Pkd1*$^{-/-}$/LZ^{+} mice. Low and Mid (intermediate) indicate the chimeric rate as estimated by coat color: Low, less than 10%; Mid, 10% to approximately 30%. (**C**) Kidneys of a P60 *Pkd1*$^{-/-}$/LZ^{+} mouse. Black arrowheads indicate hemorrhagic cysts; white arrowhead indicates pancreatic cysts. (**D**) Cross sections of kidney (Kid), liver, and pancreas (Panc) of a P60 *Pkd1*$^{-/-}$/LZ^{+} mouse. Approximately 90% of the renal parenchyma is occupied by large cysts (PAS staining). Liver and pancreas show numerous cysts (H&E). Original magnification, ×2 (kidney) and ×2.5 (liver and pancreas). (**E**) Single nephrons of *Pkd1*$^{-/-}$/LZ^{+}, *Pkd1*$^{+/-}$, and wild-type mice at E17.5. Multiple "out-pocketing" cysts are present in all segments of the nephron from the *Pkd1*$^{-/-}$/LZ^{+} mouse. Cystic dilation begins at the distal tubule of the nephron of the *Pkd1*$^{+/-}$ mouse. Scale bar: 100 μm. (**F**) Staining of a microdissected tubule with β-gal. A cystic fragment of the *Pkd1*$^{-/-}$/LZ^{+} mouse was composed of *Pkd1*$^{+/+}$ (blue; LZ^{+}) and *Pkd1*$^{+/-}$ (white; LZ^{-}) cells. Scale bar: 100 μm. (**G**) Histochemical analysis of the kidney of a *Pkd1*$^{-/-}$/LZ^{+} mouse at E17.5 with β-gal. The cyst (*) began at tubules involving *Pkd1*$^{+/-}$ (LZ^{-}) and LZ^{+} cells. Some tubules composed of LZ^{-} cells (black arrowheads) showed no cystic dilatation. Counterstaining: Nuclear Fast Red. Original magnification, ×400.

To examine dedifferentiation of flat cyst epithelial cells, we examined expression of polycystin-2 and acetylated tubulin as a marker of primary cilia in the cyst epithelial cells of *Pkd1*$^{-/-}$/LZ^{+} kidneys. All of the cyst epithelial cells expressed polycystin-2 regardless of morphological changes and *Pkd1* expression (Figure 4A), and both LZ^{+} and *Pkd1*$^{-/-}$ (LZ^{-}) cyst epithelial cells manifested cilia (Figure 4B). However, some of the cyst epithelial cells had lost expression of *Dolichos biflorus* agglutinin (DBA) lectins (Figure 4C) and Na-K ATPase (Figure 4D). The loss of expression did not correlate with loss of the *Pkd1* gene in cyst epithelial cells. The mean cell height of cyst epithelial cells with or without Na-K ATPase was lower than that of normal epithelial cells ($P < 0.001$), and the cell height of cyst epithelial cells without Na-K ATPase was slightly lower than that of cyst epithelial cells with Na-K ATPase ($P = 0.029$) (Figure 4E), indicating a tendency of correlation between the dedifferentiation and the flat shape of cyst epithelial cells.

Proliferation and apoptosis of cyst epithelial cells. Immunohistochemistry of cyst epithelial cells in *Pkd1*$^{-/-}$/LZ^{+} kidneys revealed that LZ^{+} cells occasionally showed focal hyperplastic features (Figure 5A) such as micropolyps, as observed in human ADPKD. Some of cuboidal cyst epithelial cells were accompanied by PCNA expression (Figure 5B). We investigated expression of the cell cycle regulators p21 and p53 in *Pkd1*$^{-/-}$/LZ^{+} kidneys by Western blot. Although very low expression of p21 has been reported in the whole body of *Pkd1*$^{-/-}$ embryos at E15.5 (30), the amount of p21 in the kidneys of *Pkd1*$^{-/-}$ embryos at E16.5 and *Pkd1*$^{-/-}$/LZ^{+} mice 1 month of age was slightly less than that in wild-type mice (Figure 5C). Statistical analysis of the amount of p21 in 4 independent experiments indicated a significant difference between wild-type kidneys and *Pkd1*$^{-/-}$ kidneys ($P = 0.016$) but no difference between wild-type kidneys and *Pkd1*$^{-/-}$/LZ^{+} kidneys ($P = 0.107$). Interestingly, the amount of p53 in *Pkd1*$^{-/-}$ ($P = 0.003$) and *Pkd1*$^{-/-}$/LZ^{+} ($P = 0.044$) kidneys was reduced compared with that in wild-type kidneys. Indeed, the amount of p53 decreased in the cuboidal cyst epithelial cells as well as in the flat cyst epithelial cells of *Pkd1*$^{-/-}$/LZ^{+} kidneys (Figure 5D).

To examine the proliferation of cyst epithelial cells in vitro, we cultured microdissected single nephrons with cysts from *Pkd1*$^{-/-}$/LZ^{+} kidneys in collagen gel with 10% FCS. Cells in cystically dilated parts of the nephrons rapidly proliferated in a sheet-like fashion within 18 hours (Figure 5, E–G). Although the great majority were *Pkd1*$^{-/-}$ cells, some LZ^{+} cyst epithelial cells proliferated. This significant proliferation of *Pkd1*$^{-/-}$ and LZ^{+} cyst epithelial cells was sustained by FCS, as a less significant proliferation was observed in collagen gel without FCS (data not shown).

Cyst epithelia at the early stage of cystogenesis were composed of cuboidal *Pkd1*$^{-/-}$ and LZ^{+} cells in *Pkd1*$^{-/-}$/LZ^{+} kidneys, then flat *Pkd1*$^{-/-}$ cells became dominant in cyst epithelia at the intermediate stage. As there were many apoptotic cells present in *Pkd1*$^{-/-}$/LZ^{+} kidneys at the intermediate stage (data not shown), the cuboidal LZ^{+} cells in the cyst epithelia might have been dead due to apoptosis and then filled with flat *Pkd1*$^{-/-}$ cells. Indeed, TUNEL staining of the cyst epithelial cells in *Pkd1*$^{-/-}$/LZ^{+} kidneys revealed scattered TUNEL-positive cells (Figure 6A). Apoptosis in LZ^{+} cyst epithelial cells was 3- to 4-fold larger than that in *Pkd1*$^{-/-}$ cyst epithelial cells (Figure 6B). Electron microscopic analysis of the cyst epithelia showed occasional apoptotic figures in cuboidal cells overlaid by neighboring cells (Figure 6C). In addition, flat cells overlaid several degenerated cells that were detached from the tubular basement membrane (Figure 6D), suggesting rearrangement by flat *Pkd1*$^{-/-}$ cells.

Signaling pathways in relation to proliferation or apoptosis of cyst epithelial cells. Signaling pathways related to cell proliferation were analyzed in the kidneys of *Pkd1*$^{-/-}$ and *Pkd1*$^{-/-}$/LZ^{+} mice. Phosphorylated EGFR (p-EGFR) detected in the cyst epithelial cells of *Pkd1*$^{-/-}$/LZ^{+} kidneys was significantly greater than in those of wild-type kidneys

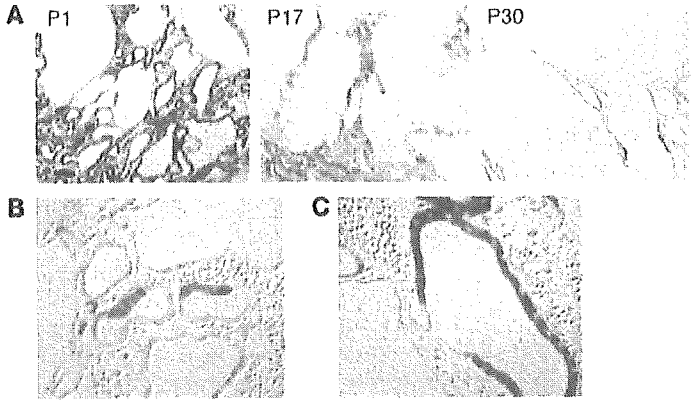

Figure 3
Histochemical analysis of *Pkd1*$^{-/-}$/LZ^{+} kidneys. Kidneys of *Pkd1*$^{-/-}$/LZ^{+} mice were stained with β-gal and counterstained with Nuclear Fast Red. (**A**) Kidneys of *Pkd1*$^{-/-}$/LZ^{+} mice with the low chimeric rate at P1, P17, and P30. At the early stage (P1), cyst epithelia were composed of *Pkd1*$^{-/-}$ (LZ^{-}) and LZ^{+} cells. At the late stage (P30), individual cysts were enlarged and most cyst epithelia were composed of *Pkd1*$^{-/-}$ (LZ^{-}) cells. Original magnification, ×200. (**B**) Kidney of a P3 *Pkd1*$^{-/-}$/LZ^{+} mouse with the intermediate chimeric rate. At the early stage of cystogenesis, both *Pkd1*$^{-/-}$ (LZ^{-}) and LZ^{+} cyst epithelial cells are cuboidal in shape. Original magnification, ×400. (**C**) Kidney of a P8 *Pkd1*$^{-/-}$/LZ^{+} mouse with the low chimeric rate. Cyst epithelia are composed of flat *Pkd1*$^{-/-}$ (LZ^{-}) cells and cuboidal LZ^{+} cells. *Pkd1*$^{-/-}$ (LZ^{-}) cyst epithelial cells changed their shape from cuboidal to flat. Original magnification, ×200.

(data not shown). To elucidate the downstream signaling pathway of growth factors, we analyzed the amount of activated MAP kinases in kidneys using Western blot and immunohistochemistry. Although the amount of p-ERK in *Pkd1*$^{-/-}$ and *Pkd1*$^{-/-}$/LZ^{+} kidneys was not different from that in wild-type kidneys (Figure 7A), expression of p-ERK was significantly more in the cyst epithelial cells of *Pkd1*$^{-/-}$/LZ^{+} kidneys regardless of their shape, cuboidal (Figure 7B) or flat (data not shown).

As for signaling pathways related to apoptosis, the amount of p-JNK was more in *Pkd1*$^{-/-}$/LZ^{+} kidneys ($P = 0.046$) but less in *Pkd1*$^{-/-}$ kidneys ($P = 0.002$) than in wild-type kidneys. Immunohistochemistry revealed that p-JNK expression was increased in the cuboidal cyst epithelial cells rather than in the flat ones of *Pkd1*$^{-/-}$/LZ^{+} kidneys, suggesting that LZ^{+} cyst epithelial cells with p-JNK expression induce apoptosis. In contrast, the amount of p-p38 in *Pkd1*$^{-/-}$/LZ^{+} and *Pkd1*$^{-/-}$ kidneys was similar to that in wild-type kidneys. Furthermore, the amount of p-Akt, an apoptotic inhibitory signal, in both *Pkd1*$^{-/-}$ ($P = 0.008$) and *Pkd1*$^{-/-}$/LZ^{+} ($P = 0.037$) kidneys was more than that in wild-type kidneys. Indeed, p-Akt expression was significantly increased in both cuboidal (data not shown) and flat cyst epithelial cells. The amount of Bcl-X_L in *Pkd1*$^{-/-}$/LZ^{+} kidneys was clearly less than that in wild-type kidneys ($P = 0.032$), whereas that in *Pkd1*$^{-/-}$ kidneys was similar to that in wild-type kidneys. The amount of Bcl-2 and Bax in *Pkd1*$^{-/-}$/LZ^{+} and *Pkd1*$^{-/-}$ kidneys was similar to that in wild-type kidneys ($P = 0.224$ and 0.821, respectively). These findings suggest that LZ^{+} cyst epithelial cells are more apoptotic than are *Pkd1*$^{-/-}$ cyst epithelial cells.

Immortalized growth of Pkd1$^{-/-}$ *mouse embryonic fibroblasts.* Most cyst epithelial cells in *Pkd1*$^{-/-}$/LZ^{+} kidneys at the late stage of cystogenesis were *Pkd1* cells, and these grew very well in collagen gel, suggesting a relationship between loss of *Pkd1* and cell immortalization. Because the 3T3 culture protocol of mouse embryonic fibroblasts (MEFs) is one of the well characterized experimental models of cell immortalization (38) and because normal MEFs express *Pkd1* (data not shown), we cultured *Pkd1*$^{-/-}$ MEFs according to the 3T3 protocol. Wild-type MEFs entered a characteristic cell cycle arrest known as cell senescence after passages 8–9 and immortalized cells (2 of 21 wells) appeared stochastically and eventually overtook the senescent cells (Figure 8A). In contrast, immortalized cells appeared in a large number of wells (21 of 24 wells) in *Pkd1*$^{-/-}$ MEF cultures, thereby suggesting a high incidence of immortalization.

Because the amount of the cell cycle regulator p16 increases in MEFs at the senescence stage (39), we analyzed expression of the cell cycle regulators p16, p21, and p53 in *Pkd1*$^{-/-}$ MEFs using Western blot. The amount of these proteins was similar in *Pkd1*$^{-/-}$ and wild-type MEFs until passage 8, whereas the amount of p16 clearly increased in both *Pkd1*$^{-/-}$ and wild-type MEFs after passage 8 (Figure 8B). However, the amount of p53 in *Pkd1*$^{-/-}$ MEFs at pas-

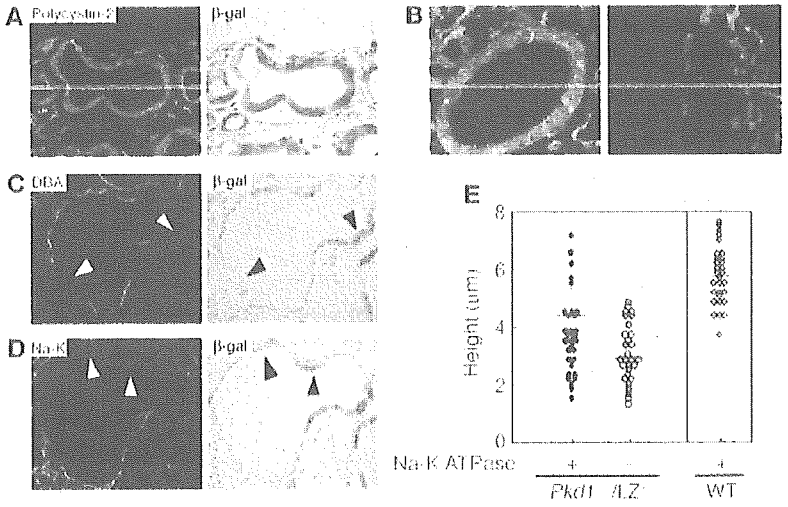

Figure 4
Dedifferentiation of *Pkd1*$^{-/-}$ cyst epithelial cells. (**A–D**) A kidney from a P8 *Pkd1*$^{-/-}$/LZ^{+} mouse was stained with anti–polycystin-2 (red, polycystin-2; blue, DAPI) (**A**), anti–acetylated tubulin (red, acetylated tubulin; green, β-gal; blue, DAPI) (**B**), anti-DBA (**C**) or anti–Na-K ATPase (**D**). (Right panels: **A**, **C**, and **D**) The same section was stained with β-gal and counterstained with Nuclear Fast Red. White and black arrowheads indicate the same epithelial cells. Original magnification, ×400. (**B**) Left and right panels indicate stainings in cuboidal and flat cyst epithelia, respectively. (**E**) Relationship between cell height and Na-K ATPase expression in the cyst epithelial cells shown in **D**. Each symbol indicates a cyst epithelial cell (*Pkd1*$^{-/-}$/LZ^{+}) or normal tubular epithelial cell (WT).

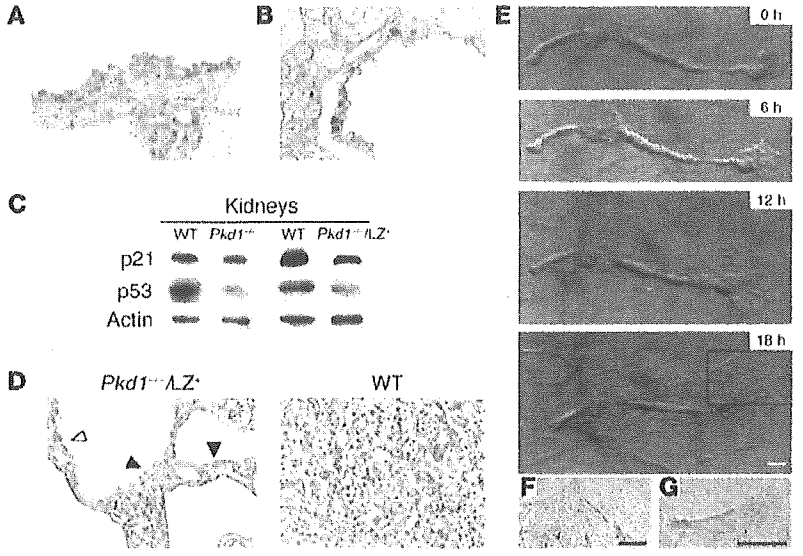

Figure 5
Proliferation of *Pkd1*$^{-/-}$ cyst epithelial cells. (**A**) A kidney from a P17 *Pkd1*$^{-/-}$/LZ^{+} mouse was stained with β-gal and counterstained with Nuclear Fast Red. LZ^{+} epithelial cells occasionally showed focal hyperplastic features such as micropolyps. Original magnification, ×400. (**B**) A kidney froma P12 *Pkd1*$^{-/-}$/LZ^{+} mouse was stained with an anti-PCNA. Some cuboidal LZ^{+} cyst epithelial cells were accompanied by PCNA expression. Original magnification, ×400. (**C**) Expression of p21 and p53 in the kidneys of *Pkd1*$^{-/-}$ mice at E16.5 and *Pkd1*$^{-/-}$/LZ^{-} mice 1 month of age. The amount of p21 and p53 in kidneys was examined using Western blot. Actin was used as a loading control for protein. Data presented are 1 representative of 4 independent experiments. (**D**) Kidneys of P12 *Pkd1*$^{-/-}$/LZ^{+} and P12 wild-type mice were stained with anti-p53. Expression of p53 was detected in the flat epithelial cells (white arrowhead) but was significantly decreased in the cuboidal cyst epithelial cells (black arrowheads) of the *Pkd1*$^{-/-}$/LZ^{+} mouse. Original magnification, ×400. (**E–G**) The proliferation of cyst epithelial cells in vitro. A single nephron isolated by microdissection from the kidney of a *Pkd1*$^{-/-}$/LZ^{+} mouse at E17.5 was cultured in collagen gel for 18 hours. (F and G) Higher magnifications of the boxed area above. Both LZ^{+} and *Pkd1*$^{-/-}$ (LZ^{-}) cells proliferated. Scale bars: 100 μm.

sage 30 ($P = 0.001$) but not that in wild-type MEFs at passage 13 ($P = 0.636$) was clearly less than that in *Pkd1*$^{-/-}$ and wild-type MEFs at passage 1. The amount of activated MAP kinases in MEFs was examined further. The amount of p-ERK in *Pkd1*$^{-/-}$ MEFs at passage 30 was slightly more than that in wild-type MEFs at passage 13. Although the amount of p-JNK ($P = 0.032$) and p-p38 ($P = 0.038$) increased in wild-type MEFs from passage 8 to passage 13, it was stable in *Pkd1*$^{-/-}$ MEFs until passage 30. The amount of p-Akt in *Pkd1*$^{-/-}$ MEFs was also stable until passage 30. Furthermore, the amount of Bcl-2 family proteins was similar in *Pkd1*$^{-/-}$ and wild-type MEFs at passages 30 and 13, respectively (data not shown).

Discussion

In the present study, we developed *Pkd1*$^{-/-}$/LZ^{+} chimeric mice. The pathological findings in *Pkd1*$^{-/-}$/LZ^{+} kidneys were similar to those in human ADPKD kidneys. Therefore, *Pkd1*$^{-/-}$/LZ^{+} mice, like *Pkd2*$^{WS25/-}$ mice (12), are a feasible model for human ADPKD. As intragenic recombination events in *Pkd2*$^{WS25/-}$ mice occurred gradually and postnatally, as in human ADPKD, whereas *Pkd1*$^{-/-}$/LZ^{+} mice have *Pkd1*$^{-/-}$ cells by inheritance, cyst formation in *Pkd1*$^{-/-}$/LZ^{+} kidneys progressed more rapidly than that in *Pkd2*$^{WS25/-}$ and human ADPKD kidneys. However, with *Pkd1*$^{-/-}$/LZ^{+} mice, we have the advantage of distinguishing *Pkd1*$^{-/-}$ cells from normal (LZ^{+}) cells and of monitoring the contribution of *Pkd1*$^{-/-}$ cells in cystogenesis. Analyses of the cyst epithelial cells in *Pkd1*$^{-/-}$/LZ^{+} kidneys can help us to understand the in vivo effect of polycystin-1 on cystogenesis.

Proliferation of normal tubular epithelial cells in early cystogenesis. Cystogenesis in human ADPKD has been proposed as being a monoclonal proliferation of PKD1- or PKD2-deficient epithelial cells (6–10). However, we found that the cystic epithelium at the early stage of cystogenesis was composed of both *Pkd1*$^{-/-}$ and LZ^{+} wild-type cells. This finding is supported by results showing that expression of polycystin-1 and polycystin-2 was detected in most cultured cells derived from ADPKD kidneys (40). We stress that the strong expression of polycystin-1 and polycystin-2 on cystic epithelia in ADPKD kidneys (31–36) may reflect involvement of normal cyst epithelial cells in the cystogenesis of human ADPKD.

The initial cystogenesis in the kidney with *Pkd1*$^{-/-}$ tubular epithelial cells requires stimulation, as some of the tubules with *Pkd1*$^{-/-}$ epithelial cells occasionally had no cystic dilatation and metanephric culture of organs harvested from *Pkd1*$^{-/-}$ mice at E13.5 failed to show cyst development (data not shown). It has been suggested that urinary flow promotes nephron development, in particular, tubular elongation with cell differentiation (41). During nephron development, it is hypothesized that the renal tubular diameter is maintained at the proper size (23) and that the primary cilium affects the maintenance of the tubular diameter by its mechanosensor function (19, 20). Cilia structure and polycystin-2 expression were manifested in the cyst epithelial cells of *Pkd1*$^{-/-}$/LZ^{+} kidneys. Thus, we surmise that polycystin-1 in the primary cilium is required for further inhibition of the proliferation of tubular epithelial cells to maintain their proper size. A *Pkd1*$^{-/-}$ epithelial cell, which is missing negative regulatory signals from polycystin-1, continuously proliferates, and this proliferation induces a "compensatory" proliferation of the surrounding normal epithelial cells in an attempt to re-establish appropriate tubular diameter and structure. This proliferation of tubular epithelial cells accounts for early cyst formation in human ADPKD.

Proliferation of Pkd1$^{-/-}$ *cyst epithelial cells.* EGFR (14, 27), cAMP (28, 29), Wnt/β-catenin (42), and p21 (30) have all been linked to the proliferation of cyst epithelial cells. However, the relationship between activation of these molecules and PKD deficiency is not clear, as those studies assumed that only *PKD*$^{-/-}$ cells proliferated in human ADPKD. Although downregulation of p21 expression in whole embryos of *Pkd1*$^{-/-}$ mice has been suggested to be involved in the proliferation of cyst epithelial cells (30) and we reproduced this downregulation in *Pkd1*$^{-/-}$ kidneys, p21 expression in *Pkd1*$^{-/-}$/LZ^{+} kidneys revealed only a slight decrease. The expression of p53 was significantly decreased in the kidneys of *Pkd1*$^{-/-}$ and *Pkd1*$^{-/-}$/LZ^{+} mice. These results support the findings that p53 expression is decreased in human embryonic kidney 293 cells with loss of polycystin-1 activity (43) and is also slightly decreased in human

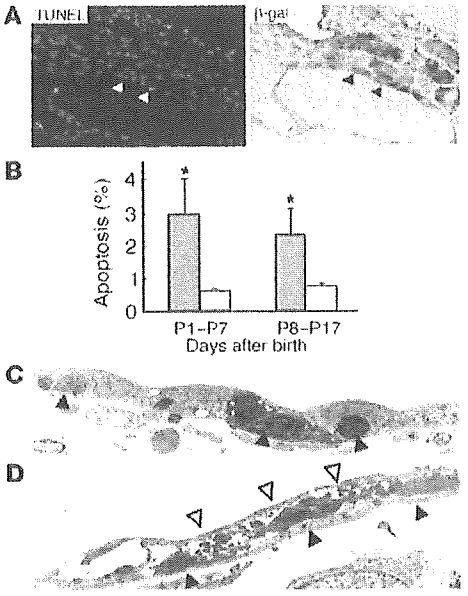

Figure 6
Apoptosis of cyst epithelial cells. (**A**) Apoptosis of cyst epithelial cells in the kidney of a P8 *Pkd1*$^{-/-}$/LZ^{+} mouse was detected by the TUNEL assay. The same section was stained with β-gal and counterstained with Nuclear Fast Red. Arrowheads indicate TUNEL-positive cells. Original magnifications, ×400. (**B**) Summary of results shown in **A**. Each graph represents the percentage of TUNEL-positive cells in LZ^{+} (black bars) and in LZ^{-} (*Pkd1*$^{-/-}$) cyst epithelial cells (white bars), respectively. The mean and SD are from 9 independent mice. $^{*}P < 0.05$. (**C** and **D**) Electron microscopic analysis of the cyst epithelium of a *Pkd1*$^{-/-}$/LZ^{+} kidney. (**C**) Occasional apoptotic cells (black arrowheads) are overlaid by neighboring cells. (**D**) Flat cells (white arrowheads) overlay several degenerated cells that are detached from the tubular basement membrane (black arrowheads). Original magnification, ×1,500.

ADPKD kidneys compared with normal kidneys (26). p53 inhibits cell cycle by induction of p21 (44), and polycystin-1 inhibits Cdk2 activity by upregulation of p21 through the activation of JAK2 (30). Thus, the decrease in p53 in addition to the lack of activation of the JAK-STAT pathway in Pkd1 deficiency may compound the decrease in p21 expression. Because expression of p53, among the cell cycle regulators examined, was affected most strongly in both *Pkd1*$^{-/-}$ cyst epithelial cells and immortalized *Pkd1*$^{-/-}$ MEFs, polycystin-1 may regulate the growth of renal tubular epithelial cells through induction of p53.

Pkd1$^{-/-}$ cyst epithelial cells were not transplantable in nude mice (data not shown). Isolated early cysts from *Pkd1*$^{-/-}$/LZ^{+} kidneys exhibited significant proliferation in vitro with 10% FCS, whereas the proliferation was stunted without FCS (data not shown), suggesting that proliferation of *Pkd1*$^{-/-}$ cyst epithelial cells is not autonomous, as in neoplasms, but instead is growth factor dependent. Among many growth factors and their receptors related with cystogenesis, strong EGFR expression was observed on cystic epithelia of *Pkd1*$^{-/-}$ kidneys (14). Interestingly, EGFR expression increased on both cuboidal and flat cyst epithelial cells in *Pkd1*$^{-/-}$/LZ^{+} kidneys (data not shown). This was supported by the finding of scattered activation of the ERK pathway in both cuboidal and flat cyst epithelial cells in *Pkd1*$^{-/-}$/LZ^{+} kidneys.

Dedifferentiation of Pkd1$^{-/-}$ *cyst epithelial cells.* The cyst epithelia in human ADPKD are composed of cuboidal cells such as normal renal epithelial cells and flat cells (24). A similar phenomenon was noted in *Pkd2*^{WS25} kidneys. These 2 morphologically different cells constitute the cyst epithelium at the early and intermediate stages of cystogenesis (45). We also detected 2 kinds of cyst epithelial cells in *Pkd1*$^{-/-}$/LZ^{+} kidneys. Both *Pkd1*$^{-/-}$ and LZ^{+} cyst epithelial cells were cuboidal in shape at the early stage of cystogenesis, and some *Pkd1*$^{-/-}$ cyst epithelial cells changed their shape to flat at the intermediate stage. As LZ^{+} cyst epithelial cells are nearly cuboidal, Pkd1 deficiency is related to the morphological change.

Most flat cyst epithelial cells are negative for nephron segment markers and Na-K ATPase (45), suggesting that the morphological transition of *Pkd1*$^{-/-}$ cyst epithelial cells is accompanied by loss of functional phenotype. However, expression of renal tubular markers within single cysts in *Pkd1*$^{-/-}$/LZ^{+} kidneys was discontinuous. Loss of expression was also detected in the cuboidal cyst epithelial cells at the early stage of cystogenesis. Although there is a tendency for correlation between loss of Na-K ATPase expression and flat shape of cyst epithelial cells, the morphological change of cyst epithelial cells is not completely correlated with the loss of tubular markers.

The cell adhesion molecules E-cadherin and β-catenin are bound to polycystin-1 and polycystin-2 (42), and E-cadherin expression decreases in *Pkd1*$^{-/-}$ kidneys (14). Thus, Pkd1 deficiency may change the polarity of cyst epithelial cells by affecting cell adhesion or

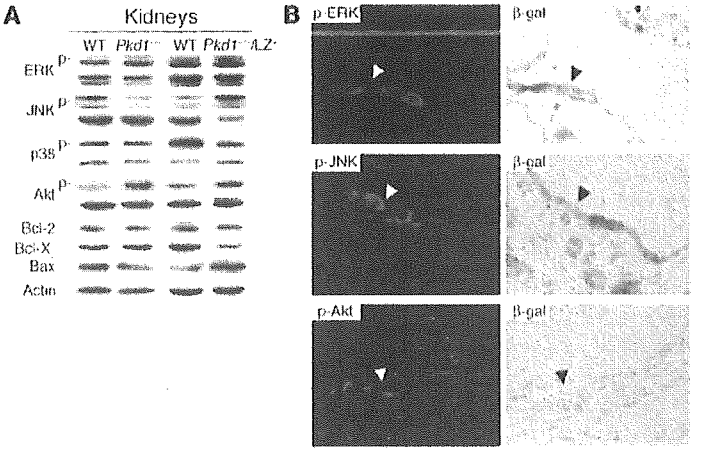

Figure 7
Signaling pathways related to proliferation or apoptosis in cyst epithelial cells. (**A**) Expression of signal transducers in the kidneys of *Pkd1*$^{-/-}$ mice at E16.5 and *Pkd1*$^{-/-}$/LZ^{+} mice 1 month of age was analyzed using Western blot. Actin was used as a loading control for protein. Data presented are 1 representative of 4 independent experiments. (**B**) A kidney from a P8 *Pkd1*$^{-/-}$/LZ^{+} mouse was stained with anti–p-ERK, anti–p-JNK, or anti–p-Akt. The same section was stained with β-gal and counterstained with Nuclear Fast Red. Black and white arrowheads indicate the same epithelial cells. Original magnification, ×400.